https://doi.org/10.5194/egusphere-2026-1504
Preprint. Discussion started: 18 May 2026

A data assimilation scheme to improve groundwater state estimation in the Aqui-FR modelling platform

Adrien Manlay[1,2], Jean-Pierre Vergnes[1], Simon Munier[3], and Florence Habets[2]

[1]BRGM - French Geological Survey, F-45060 Orléans, France
[2]Laboratory of Geology - École Normale Supérieure, PSL University, Institut Pierre Simon Laplace, CNRS UMR 8538, F-75005 Paris, France
[3]Météo-France, CNRS, Univ. Toulouse, CNRM, Toulouse, France

Correspondence: Adrien Manlay (a.manlay@brgm.fr)

Abstract.

Groundwater is a key resource for human activities, and anticipating its evolutions months in advance is a major challenge for stakeholders. Hydrological model for subsurface flows can be used for groundwater level forecasts. However, due to uncertainties in the model's forcings and parameters, forecast initial state estimation may be inaccurate. We propose the implementation of a sequential data assimilation (DA) scheme within the Aqui-FR modelling platform, aiming at improving groundwater state estimation over a regional scale for future seasonal forecasting system. We assimilated in situ groundwater level observations into a regional hydrogeological model, using a Localized Ensemble Kalman Filter (LEnKF). Two localization methods are assessed to evaluate the best way to propagate data assimilation increment from observation sites into the model space. A distance based method is compared to a correlation method, based on a variogram analysis. Both method show good performances to improve groundwater head simulations, with a root-mean-square error (RMSE) reduction of 90% compared to a reference simulation without DA [open loop (OL) run]. Experiments with validation observations sites show that the correlation method lead to a more robust DA analysis, with less degradation of the simulation compared to OL run and measurements. Hindcast experiments using reanalysis of atmospheric forcing suggest that state assimilation, in context of inertial aquifers, can help improve forecast within a six-month range. The persistence of DA correction varies within the model space domain and may be due by an initial calibration that could be improved. After a three months lead time, 75% of assimilated observation sites still show an improvement of RMSE compared to OL.

1 Introduction

Around the world, groundwater is used extensively for human activities, with many people relying on it for drinking water, agriculture or industrial uses (Wada et al., 2010, 2014). Groundwater is used to provide approximately two-thirds of France's drinking water (Maréchal and Rouillard, 2020). In the last decade, Europe, and especially France, has faced several severe droughts (Rakovec et al., 2022; Tripathy and Mishra, 2023; Albergel et al., 2019), that can affect different component of the water cycle, from atmospheric variables to groundwater (Van Loon et al., 2012), and impact many activities (Stahl et al., 2016;

https://doi.org/10.5194/egusphere-2026-1504
Preprint. Discussion started: 18 May 2026

Biella et al., 2024). Thus, anticipating groundwater deficit or the duration of flood risk due to high groundwater level months in advance is a major challenge for stakeholders.

Over the last two decades, different hydrological seasonal forecasting systems have introduced (e.g., Ramos et al., 2007), but only a limited number of papers have included groundwater (e.g., Wanders et al., 2019; Getirana et al., 2020; Belleflamme et al., 2023). Groundwater level estimation remains challenging because of the uncertainties on unobserved properties of the subsurface governing underground diffusive flows. To avoid the difficulties associated with spatially distributed models, few hydrological forecasting used conceptual lumped model to provide seasonal outlook of groundwater levels, either with atmospheric ensemble seasonal forecasts as forcing (Mackay et al., 2015; Prudhomme et al., 2017) or with historical climatic forecasting (Surdyk et al., 2022). Recently, machine learning models have also become increasingly popular (Boo et al., 2024).

Nevertheless, recently, spatially distributed and integrated models, with surface and subsurface representations, are also increasingly used (Dasgupta et al., 2022), in order to improve the spatial coverage of such tools. For example, in Germany a groundwater forecasting system based on distributed physical model with Parflow/CLM (Belleflamme et al., 2023) has been developed, using a 0.6 km spatial resolution and an hourly simulation time steps, solving Richards equation. In the United States, Getirana et al. (2020) employed a Land-Surface Model (LSM) including a simplified representation of groundwater flows but showing great results during hindcast compared to in situ observations. In France, the Aqui-FR hydrometeorological system (Vergnes et al., 2020) is also used for seasonal forecast. The use of regional groundwater models coupled to atmospheric seasonal forecast and LSM show great perspective for forecasting the spatial and temporal evolution of groundwater at spatial scale of decision-making. Nevertheless, the role of initial hydrological conditions (IHC) have shown to have great impact on forecast (Li et al., 2009; Shukla and Lettenmaier, 2011) and especially the groundwater initial state (Wanders et al., 2019; He et al., 2019). Indeed, generally speaking, regional groundwater models used parameters calibrated against observed groundwater level time series over a time windows spanning several months or years. While such calibration increases confidence in the models, uncertainties associated with model errors still persist (Hendricks Franssen and Kinzelbach, 2009; Wanders et al., 2019). These uncertainties can spread to the forecast and hence diminishes its performances, and motivating the adoption of data assimilation in hydrogeological models to reduce prediction biases and uncertainties (Doherty and Moore, 2020; Camporese and Girotto, 2022).

Data assimilation consist in optimal combination of both observations and a model representation of a physical system in order to improve the latter. Various methods have been explored in meteorology, oceanography from minimum variance approach to variational algorithms (Carrassi et al., 2018), with Bayesian based method. The underlying method is based on the BLUE (Best Linear Unbiased Estimator) and the Kalman filter (KF). The most widely used technique is the EnKF (Ensemble Kalman Filter), designed as a Monte Carlo implementation of the KF by Evensen (1994) and modified by (Burgers et al., 1998).

For groundwater, numerous studies that include data assimilation in distributed models focus on parameter estimation in history matching and inverse modelling (e.g., de Marsily et al., 2000; Zhou et al., 2014; White, 2018). Nevertheless, considering a long period for history matching, the estimated parameters can be smoothed to fit over different hydrological conditions and not be good enough for IHC estimation (Hendricks Franssen and Kinzelbach, 2008). For a forecasting application, Wanders

https://doi.org/10.5194/egusphere-2026-1504
Preprint. Discussion started: 18 May 2026

et al. (2019) demonstrated that, in the case of groundwater, the forecast initial conditions are crucial due to inertial dynamics within a prediction range of three months, and thus require a particular attention. Recently sequential DA have been introduced in inverse modelling tools used in the groundwater community (Alzraiee et al., 2022) and groundwater models have been coupled to DA tools (Tang et al., 2024), thus gathering similar methods to achieve these different goals.

Sequential data assimilation is thus used for real-time modelling and forecasting. Hendricks Franssen and Kinzelbach (2008) used a dual state and parameter estimation with an EnKF and an "augmented state vector" method for real time modelling. The authors showed the efficiency of ensemble methods on a synthetic case by comparing different implementations of the determinist variant of EnKF, with varying spatial and temporal observations. Here, large ensemble have been used for a better statistical estimation of the empirical covariances from the ensemble.

This method was also used for a real-case at local scale by Hendricks Franssen et al. (2011) who compares performances between state DA and dual state and parameter DA. It was shown that state DA can improve groundwater level estimation, with a correction persistence up to ten days. Beyond this range, dual state-parameter DA outperforms state only DA, suggesting that model trajectory are more influenced by parameter than initial state. Nevertheless, model errors were still lower than no DA runs for 500 days after a forecast initialization with a synthetic model, and benefits of DA were still visible after 10 days with a real-world case.

Over the past decade, various strategies have been explored for optimizing the DA workflow. Zhang et al. (2015) show that, depending on the observation spatial density, the ensemble size could be reduced (90 to 30 members) without degrading DA performance. The authors also concluded about the importance of model's error estimation, even if it is overestimated. In a further study, Zhang et al. (2016) used a multivariate DA workflow to assimilate both soil moisture and groundwater head in a hydrogeological model, with explicit unsaturated zone representation. The authors showed mitigated results, or even degradation of the simulations, when assimilating one variable and measuring the impact one the other. He et al. (2019) also used a multivariate DA workflow, with assimilation of river discharge and groundwater levels. In this case, the DA increment calculated from one state variable analysis was restricted to prevent impact on the other variable and keep efficiency on both variables. This setup was used for hindcast experiments of short range forecast (48h of lead time), showing that state estimation for groundwater head was crucial for the forecast efficiency. Other authors also suggested that multivariate DA does not always improve both variable simulations (e.g., Camporese et al., 2009; Rasmussen et al., 2016; Botto et al., 2018), even with integrated models. Multivariate DA in different component of coupled model is even more challenging (Camporese and Girotto, 2022), although possible (Thirel et al., 2010). Consequently, the focus of assimilation may initially be on the variable to be predicted.

Most of the studies cited used synthetic cases or local scale real cases. The use of DA within integrated models (coupling surface and subsurface processes) models open the way for a change of spatial scale for groundwater (Kurtz et al., 2016; Getirana et al., 2020; Hung et al., 2022; Li et al., 2023; Tang et al., 2024). Nevertheless, this change in scale also involves a higher computational burden for both model runs and DA analysis, which motivates the use of smaller ensemble. In EnKF-based methods, long range spurious correlation arises in empirical covariances matrices from reduced size ensemble (Hamill et al., 2001; Ehrendorfer, 2007). Localization techniques are often used to dampen such erroneous correlations (Ehrendorfer, 2007; Morzfeld and Hodyss, 2023). For example, Hung et al. (2022) performed groundwater levels and soil moisture DA into

https://doi.org/10.5194/egusphere-2026-1504
Preprint. Discussion started: 18 May 2026

a Parflow/CLM model with a Localized EnKF (LEnKF), using distance based localization (i.e. correlations in covariances are reduced with respect to the distance to observations, using a quasi Gaussian function from 0 to 1). In this study, a domain of 57,850 km^2 was used with cells of 800 m resolution. The authors managed to improve groundwater estimations with state DA and dual state-parameter DA for a basin of 13,928 km^2 in this domain, using twin experiments. Li et al. (2023) applied a similar methodology at a smaller scale (2,000 km^2) but using real-case settings and observations. They show more limited improvements on state estimation but still encouraging results. The computational burden of such tools is still very high (Hung et al., 2022; Li et al., 2023),potentially limiting outlooks for operational uses. On the other hand, Getirana et al. (2020) used a LSM and Gravity Recovery and Climate Experiment data assimilation (GRACE-DA, based on Ensemble Kalman Smoother) to improve groundwater state estimation and forecast (with a 3 months range) across the United States, with satellite-based terrestrial water storage (TWS) estimation. Their results show good performance of GRACE-DA to reduce forecast error in hindcast experiments, compared to in situ observations at wells. Lower improvements of the forecast system were found in region influenced by groundwater abstractions, which was not accounted for in the LSM used. The use of satellite-based data, continuous in space, lower the need for localization in the EnKF-like methods. But regarding the spatial resolution (e.g. for GRACE from 1°to 2°), using these products is still limited to large scale model. For regional studies, it is required to enhance the accuracy of GRACE products, for example with downscaling methods or global data assimilation systems (Houborg et al., 2012; Pascal et al., 2022; Guardiola-Albert et al., 2024).

For real cases applications, with spatially sparse data and at basin or regional scale, the parametrization of DA schemes in hydrogeology is thus still very challenging. Localization, even simple or limited, seems to be a crucial point for effective DA (Morzfeld and Hodyss, 2023), and can help reduce the ensemble size (Zhang et al., 2016) (and thus, the computational burden). Distance based method are often used (e.g., Zhang et al., 2016; Li et al., 2023), but required to fix a maximum distance to cut correlations. This distance can be set with a variographic analysis (Li et al., 2023). DA efficiency can be sensitive to this parameter, and using a constant distance for every observation may not be optimal. Moreover, using a circular influence of observations in space is suitable for atmospheric or ocean physics but can be improved for hydrological problems, especially in case of unconfined groundwater modelling. Thus, adaptative localization methods has emerged in hydrogeology to overcome these difficulties (e.g., Anderson, 2007; Rasmussen et al., 2015; Luo and Bhakta, 2020). Rasmussen et al. (2015) used a correlation between each cell of every ensemble member and each observed cells to define a localization matrix. Such methods improve the spatial pattern of the localization matrix and DA efficiency, especially for reduced ensemble size or low observation density in groundwater models (Rasmussen et al., 2015). Nevertheless, the localization is computed at each assimilation step and requires a large amount of ensemble members to be efficient (Luo and Bhakta, 2020), which can be computationally expensive. In surface large scale hydrology, an adaptive method based on semi-empirical patches has been developed (Revel et al., 2019). It is based on a variographic analysis of model space and can integrate time dynamics. The principal benefit of this approach is that it enables the identification of a physical pattern of the model and use it to propagate DA correction. The authors show improvement in DA efficiency when assimilating satellite based observations into land surface models. The localization matrix can be computed as a preprocessing step, and available for every DA cycle. However, this method has not yet been implemented or tested for a regional-scale groundwater model.

https://doi.org/10.5194/egusphere-2026-1504
Preprint. Discussion started: 18 May 2026

This research present the implementation of a sequential data assimilation scheme within the workflow of the Aqui-FR modelling platform, and its evaluation over a hydrogeological regional parts of this platform. Different localization methods are assessed to evaluate the best way to propagate DA increment from in situ observation at well location into the model space. The variogram (or correlation) based localization is investigated, compared to the distance based one. Different experiments are conducted to evaluate the potential of such method for groundwater seasonal forecasts, using hindcast simulations with atmospheric reanalysis. The details about the model used, the DA scheme and the experiments are described in the methodology section (2). The results of the evaluation of the DA scheme, compared to a reference simulation and observations, are presented in section 3 and discussed in section 4, before the conclusions.

2 Materials and methods

2.1 Hydrometeorological modelling

The Aqui-FR hydrometeorological modelling chain (Vergnes et al., 2020) gather different hydrological codes and models, aiming at providing real-time modelling and seasonal forecasts of groundwater levels at regional scale over France. The modelling chain is composed of three main components: the meteorological forcing (SAFRAN reanalysis, Quintana-Seguí et al., 2008; Vidal et al., 2010), a land surface model (ISBA from the Surfex platform, Masson et al., 2013; Le Moigne et al., 2020) for surface water balance, and hydrological models (Vergnes et al., 2020) for surface and subsurface water flows.

At each time step, the platform uses the run-off and infiltration fluxes computed by the ISBA component and send them to the hydrological models that simulate the flow through the unsaturated zone, the river discharge, the groundwater flows and the rivers-groundwater exchanges. In version 1.4, the coupling of ISBA with the hydrological models neglects any feedback from groundwater to the soil. Two hydrological computer codes are included, the MARTHE model (Thiéry, 2013; Thiéry et al., 2018, 2020) ("Modélisation des Aquifères avec un maillage Rectangulaire, Transport et HydrodynamiquE" in French) and the EauDyssée model (Saleh et al., 2011). A conceptual lumped model, Eros (Thiéry and Moutzopoulos, 1992; Thiéry, 2018), is also included to simulate karstic springs. In this study, only the MARTHE computer code was used. It uses a 3-dimensional finite volume numerical scheme (Thiéry, 2013) to solve groundwater flow diffusion equations (de Marsily, 1986). This numerical scheme is fully coupled to a simplified kinetic wave approach to compute river flows. The MARTHE code is detailed by Thiéry et al. (2020).

About one third of the French national territory is covered by the Aqui-FR platform, with different applications of the MARTHE and EauDyssée codes at regional scale. The spatial coverage is described by Vergnes et al. (2020). In version 1.4, Aqui-FR gather 14 spatially distributed models, single or multi layer, with a grid cell sizes varying from 100 m to 2 km. The platform simulates groundwater and river flows a time step of 1 day and has been evaluated through a 60-year retrospective simulation (Vergnes et al., 2020) showing good results for long term impact studies and operational uses, regarding model uncertainties. The Aqui-FR platform is used for real-time modelling, seasonal forecasts (Leroux et al., 2019; Willemet et al., 2022) and scientific studies (e.g. wetland evaluation, Guillaumot et al. (2024); climate change studies, Jeantet et al. (2025)).

https://doi.org/10.5194/egusphere-2026-1504
Preprint. Discussion started: 18 May 2026

2.2 Study area

The different experiments are conducted within a subdomain of Aqui-FR modelling chain. The study area focus on the Somme basin (6,568 km^2), located in northern France (Fig. 1). The topography is quite smooth, varying from 218 to 0 m a.s.l. The Somme river rises at 88 m a.s.l and flows from east to west for approximately 245 km before emptying in the sea (the Channel). Its average monthly mean discharge is about 35.2 $m^3.s^{-1}$ near its outlet (gauging station E647 0910, https://hydro.eaufrance.fr/sitehydro/E6470910/synthese, last access: 2026-05-06). The river discharge is strongly supported by the Chalk unconfined aquifer (Pinault et al., 2005; Habets et al., 2010), which has led to groundwater-induced flooding in 2001.

The principal aquifer consists of chalk deposits from the late Cretaceous period (Turonian to Campanian stages). It is characterized by a dual porosity (West et al., 2023); itself composed of a matrix porosity, that contribute to the storage capacity, and fractures that contribute to the groundwater kinetic (Price et al., 2000). Unlike other chalk catchment (e.g. for France in Normandy), there is no evidence of karstic dynamics in the Somme basin. The lower boundary of the aquifer is composed of Early and Middle Turonian marl. Quaternary deposits are also present: alluvium can be found in riverbed, while silt is present in the hills. In the valleys, water table is equivalent between alluvium and chalk aquifers.

The total thickness of the aquifer ranges from 20 to 200 metres, but the productivity is essentially ensured by the first few metres (20-30 m), which are more fissured. The fissuring of the chalk is related to distance to the riverbed. A higher density of fractures has been identified in the areas near to the river, with a lower density found in the hills. The unsaturated zone (UZ) follow the same pattern of spatial variation with a range from 1 m near the rivers to more than 50 m in the hills (Habets et al., 2010). Due to this dual porosity, the UZ and its spatial distribution, the aquifer reacts non-linearly to climatic forcings in the catchment (Pinault et al., 2005; Habets et al., 2010). Influenced by a pluvial oceanic regime, and large scale climate drivers, groundwater dynamics exhibit multi-timescale patterns, with major contribution of the low-frequency cycles (multiannual) component over the annual/seasonal signal (Baulon et al., 2022, 2025). An example of simulated/observed time series and associated frequencies is shown in Appendix A1.

The regional hydrogeological model of the Somme, included in Aqui-FR, covers an area of 7527 km^2, larger than the physiographic catchment to include more realistic lateral boundaries. The domain is composed of a single aquifer layer of 66,924 cells with a spatial resolution varying from 500 m in the plateau/hills, to 100 m in the valley, near the river (Amraoui et al., 2002; Habets et al., 2010). The Somme river and its tributaries are explicitly represented. The initial hydraulic conductivity was derived from UZ thickness interpolation and pumping test data analysis (Amraoui et al., 2002). The model is built with the MARTHE code (Thiéry, 2013; Thiéry et al., 2020), described in the previous section, for solving river and groundwater flow equations. Vertical flows through UZ are not explicitly modelled. UZ is represented with a conceptual approach (based on the lumped model Gardénia, Thiéry (1988), included in MARTHE) used as a transfer function for forcings.

2.3 Ensemble Kalman Filter

Numerous methods exist for data assimilation, from variational implementation to Bayesian and minimum variance approaches (Carrassi et al., 2018). In hydrology, the Ensemble Kalman Filter (EnKF, Evensen, 1994; Burgers et al., 1998) and associated

https://doi.org/10.5194/egusphere-2026-1504
Preprint. Discussion started: 18 May 2026

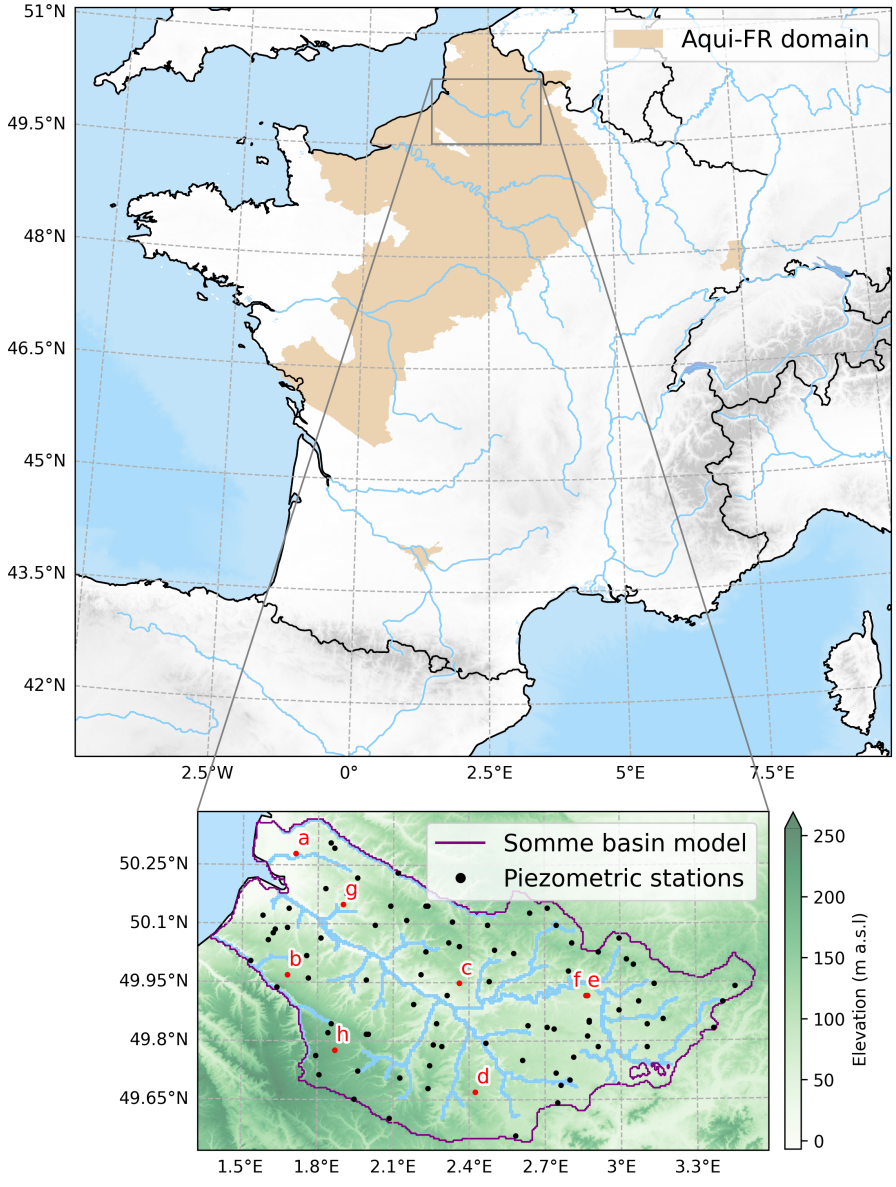

Figure 1. Localization of the study zone. The Aqui-FR domain is represented as a grey polygon. The Somme and the main river network are shown in blue in the zoom and the extension of the MARTHE model used is represented as a purple line. The location of groundwater observation sites used in this study are shown as black dots. Red dots indicate the observations sites selected for time series analysis in section 3 and the associated letters correspond to the subplots in Fig. 4. Elevation data (in meters above sea level) from the NASA Shuttle Radar Topography Mission (SRTM) data (Farr et al., 2007) are used.

methods (e.g. Ensemble Square Root Filter, Singular Evolutive Interpolated Kalman filter) have shown good performance in

https://doi.org/10.5194/egusphere-2026-1504
Preprint. Discussion started: 18 May 2026

various applications (e.g., Sun et al., 2016). The EnKF is a sequential DA scheme where state (and/or parameters) are updated using a Monte Carlo estimation of the covariances required in the Kalman filter algorithm, making it suitable for large scale models without the need for linearization of the model and the observation operator, which is responsible for mapping the model variables to the observation space.

Here, we used a stochastic sequential implementation of the EnKF, with localization (LEnKF). With m being the dimension of the state variable (groundwater head here), p the dimension of observations, and k the dimension of ensemble members (or realizations), the $m \times k$ forecast ensemble matrix $\mathbf{x}^f$ is updated using the $p \times k$ perturbed observations ensemble matrix $\mathbf{y}^o$, the $p \times k$ observation operator ensemble matrix $\mathcal{H}(\mathbf{x}^f)$, and the $p \times p$ observation error covariance matrix $\mathbf{R}$. The state variable is updated ($\mathbf{x}^a$) during the analysis step, given by (Carrassi et al., 2018):

$$\mathbf{x}^a = \mathbf{x}^f + \mathbf{K}\left[\mathbf{y}^o - \mathcal{H}(\mathbf{x}^f)\right] \tag{1}$$

With $\mathbf{K}$ the Kalman gain matrix computed as follows (Carrassi et al., 2018):

$$\mathbf{K} = \mathbf{P}^f\mathbf{H}^\top\left(\mathbf{H}\mathbf{P}^f\mathbf{H}^\top + \mathbf{R}\right)^{-1} \tag{2}$$

Where $\mathbf{P}^f$ is the forecast error covariance matrix, and $\mathbf{H}$ is the tangent linear of the observation operator.

The observation covariance $\mathbf{HPH}^\top$ and the cross covariance $\mathbf{PH}^\top$ are estimated using the ensemble, thus avoiding the need for the tangent linear operator, as follows:

$$\mathbf{PH}^\top = \frac{1}{k-1}\sum_{i=1}^{k}\left(\mathbf{x}_i^f - \langle\mathbf{x}\rangle\right)\left[\mathcal{H}(\mathbf{x}_i^f) - \langle\mathbf{x}\rangle\right]^\top \tag{3}$$

$$\mathbf{HPH}^\top = \frac{1}{k-1}\sum_{i=1}^{k}\left[\mathcal{H}(\mathbf{x}_i^f) - \langle\mathcal{H}(\mathbf{x}^f)\rangle\right]\left[\mathcal{H}(\mathbf{x}_i^f) - \langle\mathcal{H}(\mathbf{x}^f)\rangle\right]^\top \tag{4}$$

Finally, the analysis is assessed by averaging the updated ensemble members and then send to a main additional realization (no perturbed). The ensemble is propagated through the hydrological model (that we can note $\mathcal{M}$, corresponding to the Marthe model here) until next assimilation cycle.

This scheme was implemented as a Python library (Manlay, 2026), used within the Aqui-FR framework. During a simulation, the Aqui-FR driver gets the simulated variables from the hydrological models and then send them to the assimilation code which perform the DA step before sending back the analysis, through MPI (Message Passing Interface) communications. The MARTHE code has been slightly modified to allow this online sequential DA scheme. This workflow requires $k+1$ runs of the model (ensemble and main model) and $k+4$ tasks in total for the Aqui-FR driver, the assimilation code, the post-processing (I/O) task and the ensemble/main model runs.

2.4 Localization and inflation

With a finite ensemble size, the EnKF algorithm is subject to two key issues (Ehrendorfer, 2007). Firstly, sampling errors in the estimated empirical covariances can lead to erroneous ("spurious long-range") correlations (Hamill et al., 2001; Houtekamer

https://doi.org/10.5194/egusphere-2026-1504
Preprint. Discussion started: 18 May 2026

and Mitchell, 2001). Moreover, the statistical depletion of the sample can lead to filter collapse (Hamill et al., 2001; Anderson, 2001), where the ensemble standard deviation is underestimated, and the analysis step is not efficient. These limitations are often overcome using inflation and localization (Ehrendorfer, 2007; Morzfeld and Hodyss, 2023).

2.4.1 Localization

The main purpose of localization is to dampen spurious long-range correlations (Morzfeld and Hodyss, 2023). In this study we use two different localization methods: the classical "Gaspari and Cohn" quasi-Gaussian function (Gaspari and Cohn, 1999), and a variogram (or correlation) based method developed for surface hydrology (Revel et al., 2019).

For the Gaspari and Cohn (GC) method, a fifth order function of the distance d_{ij} between two points i and j defines a localization weight w_{ij} (Gaspari and Cohn, 1999):

$$w_{ij} = \begin{cases} -\frac{1}{4}z^5 + \frac{1}{2}z^4 + \frac{5}{8}z^3 - \frac{5}{3}z^2 + 1 & \text{if } z \leq 1 \\ \frac{1}{12}z^5 - \frac{1}{2}z^4 + \frac{5}{8}z^3 + \frac{5}{3}z^2 - 5z + 4 - \frac{2}{3}\frac{1}{z} & \text{if } 1 < z \leq 2 \\ 0 & \text{else } z > 2 \end{cases} \tag{5}$$

With $z = \frac{d_{ij}}{r}$ where r is the radius, i.e. the distance at which the covariance is reduced to 0, and d the distance. A good estimation of z is crucial for effective assimilation (Li et al., 2023). Here, the distance d_{ij} is computed as the Euclidean distance between the current cell i and the target cell j and the radius r is set to 12 km, based on a variographic analysis of the model space. The resulting weight matrix $\mathbf{L}$, composed of w_{ij}, vary between 0 and 1, and have the same dimension as the covariance matrix to be regularized ($\mathbf{PH}^\top$ or $\mathbf{HPH}^\top$). This matrix is then used to dampen covariances noises using a Schur (Hadamard, i.e. element by element, noted as $\circ$) product (Hamill et al., 2001; Houtekamer and Mitchell, 2001).

For the variogram method (Revel et al., 2019), we computed an experimental semi-variogram (SVG, γ) in the cross space (state and observation), i.e. for each observation the semi-variance is computed between the current cell (i) time series and every other cells (j) time series in the state domain (Eq 6). Semi-variance is computed between two cells with monthly average time series of open-loop simulation (from 1991 to 2024). A variogram model is fitted over this experimental semi-variogram, using a least-square algorithm. The best model, between Gaussian, spheric and exponential, is chosen based on RMSE against experimental SVG and used to extract variogram parameters (nugget, sill, range). Then the autocorrelation function is computed by inverting the SVG and normalizing with the sill (Eq. 7). A threshold is used to dampen non-significant correlations. After manual tuning, we opted for 0.7 as the threshold, which closely matches the value (0.6) used by (Revel et al., 2019). The localization matrix is then defined by this autocorrelation coefficient, clipped with the chosen threshold, where values are set to 0, and weighted based on distance to observation, as in GC method. This matrix is computed in a preprocessing step, for all possible observations locations, and stored. In the sequential DA, the total matrix (of shape (m, p)) is subset with observations used during the current assimilation cycle.

$$\gamma_{i,j} = \frac{1}{2N_t} \sum_{t=1}^{N_t} \left| z_{i,t} - z_{j,t} \right|^2 \tag{6}$$

https://doi.org/10.5194/egusphere-2026-1504
Preprint. Discussion started: 18 May 2026

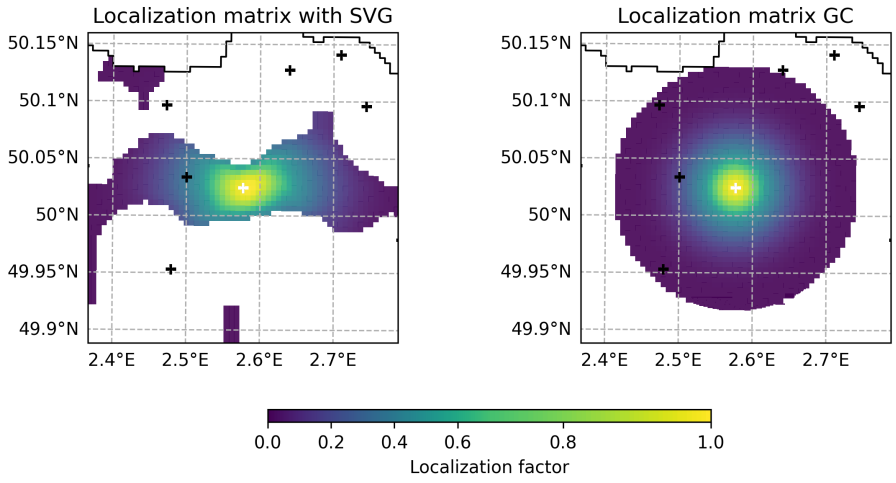

Figure 2. Comparison of spatial correlation pattern between variogram (SVG) and distance based method (GC) for localization. Observations location are represented as black cross, and the white cross indicate current observation.

$$ACF = 1 - \frac{\gamma_{i,j}}{sill} \tag{7}$$

For each method, weight matrices $\mathbf{L}$ are computed and applied to the covariance matrices $\mathbf{PH}^\top$ and $\mathbf{HPH}^\top$. The analysis equation (1), with the Kalman gain (eq. 2), then becomes:

$$\mathbf{x}^a = \mathbf{x}^f + \mathbf{L}_{xy} \circ \mathbf{PH}^\top \left(\mathbf{L}_{yy} \circ \mathbf{HPH}^\top + \mathbf{R} \right)^{-1} \left[\mathbf{y}^o - \mathcal{H}(\mathbf{x}^f) \right] \tag{8}$$

Where $\mathbf{L}_{xy}$ is the localization matrix in cross space (state $\times$ observation dimension, hence with $m \times p$ size, as $\mathbf{PH}^\top$) and $\mathbf{L}_{yy}$ is the localization matrix in observation space ($p \times p$ dimensions, as $\mathbf{HPH}^\top$).

An example of comparison between the two correlation maps is illustrated in Fig. 2. The variogram method does not always increase localization distance but allow including more physical patterns into the localization matrix.

2.4.2 Inflation

Inflation method is used to prevent filter collapse (Ehrendorfer, 2007; Carrassi et al., 2018). The multiplicative inflation we used, with an adaptive inflation factor λ_i, is adapted from the methodology of Rasmussen et al. (2015), and computed as the ratio between an objective ensemble spread and the actual ensemble spread (Eq. 9). Here, the objective ensemble spread is set based on the observation error covariance as the goal of inflation is to keep the background spread greater than the observation spread.

$$\lambda_i = \frac{\sigma_{\mathbf{R}_i}}{\sigma_{\mathcal{H}(x_i)}} \tag{9}$$

https://doi.org/10.5194/egusphere-2026-1504
Preprint. Discussion started: 18 May 2026

Where $\sigma_{\mathcal{H}(x_i)}$ and $\sigma_{\mathbf{R}_i}$ are the ensemble standard deviation and the observation error standard deviation for the i^{th} observation, respectively.

Ensemble anomalies are then multiplied by the inflation factor in order to rescale the standard deviation of the ensemble for the next assimilation cycle :

$$\mathbf{x_{infl}} = \overline{\mathbf{x}^a} + \lambda(\mathbf{x}^a - \overline{\mathbf{x}^a}) \tag{10}$$

As Rasmussen et al. (2015) suggested, inflation only applies if the standard deviation of the analysed ensemble is below a target level, defined as 20% of the initial perturbed ensemble spread. This mask is applied cell by cell to allow maintaining a sufficient local spread in the ensemble while avoiding instabilities in areas where the standard deviation was sufficient. The algorithm was also modified to allow more spatial adaptation of inflation, using the $\mathbf{L}_{xy}$ location matrix as a boolean factor. The Schur product of this boolean mask matrix with the inflated ensemble ensure that only cells affected by data assimilation updates are actually inflated.

2.5 Experiments configuration

2.5.1 Data set and observation error

In situ measurements are available over the study area and assimilated. The observation dataset is fetched from ADES French database (https://ades.eaufrance.fr/, Winckel et al., 2022), which gather groundwater level observations from national piezometric monitoring network. Water levels are expressed as meters above sea level (m a.s.l.). Data are collected with HubEau API (https://hubeau.eaufrance.fr/page/api-piezometrie) and Python requests over the study area. 387 observations stations are available within the study area, with data available from 1991 to 2024 and at least one year of data and 12 measurements. Following a similar method as described by Baulon et al. (2022), 91 stations are chosen, based on statistical criteria (length of time series and minimum frequency of data), data quality filtering (removal of data influenced by withdrawal, drought and data tagged as incorrect) and manual verification of the data quality. Observations are not always available at all stations for each data assimilation cycle. On average, about 50 observations stations are assimilated at the same time.

The observation operator involves the linear extraction of the simulated groundwater levels at the observed grid cells. Hence, the $\mathbf{H}$ matrix of Eq. 1 correspond to the identity matrix.

The observation uncertainty is estimated to mimic the known error of the pressure sensor measuring in situ groundwater level. This error is usually a few percent of the measurable variation. This range is unfortunately unknown in public databases. Therefore, a theoretical average percentage was chosen and set to 2%. The observation uncertainty is then computed for each station to 2% of the maximum range of observed data.

2.5.2 Ensemble generation

As the EnKF is a Monte Carlo approximation of the Kalman Filter, the ensemble should represent the uncertainty of the model for proper update step. With more ensemble members (or realizations), the EnKF is expected to provide better estimates of

https://doi.org/10.5194/egusphere-2026-1504
Preprint. Discussion started: 18 May 2026

statistics and empirical covariances, whilst increasing the computational burden. Hendricks Franssen and Kinzelbach (2008) stated that an ensemble of 100 members should be sufficient for state updating applied to groundwater modelling. For example, Li et al. (2023) used 128 realizations. After different configurations test (10, 25, 50, 100), an ensemble with 50 members is used. This set up showed good performances, with less computational burden than large ensemble (100 or more members).

As uncertainty in state estimation comes from forcings, initial state and parameters, the generation of the ensemble involved the perturbation of both meteorological forcings and initial states. Parameters were not directly perturbed as they are not updated in the analysis steps. In Aqui-FR modelling platform, forcings for groundwater models are the output run-off and infiltration from ISBA LSM, forced with SAFRAN meteorological reanalysis. These fluxes were perturbed using a Gaussian noise, sampled from a standard deviation (Piazzi et al., 2021), along a first-order autoregressive model (FOAR) for time dependant perturbations, following the method described by Evensen (2003) and Clark et al. (2008). The temporal scale for the FOAR model is assessed from a preprocessing step, using an autocorrelation estimation of the forcings time series. The timescales used for the run-off and infiltration are 1 and 12 days, respectively. These parameters are estimated based on the time lag at which the autocorrelation value falls below 0.8. In addition, the spatial autocorrelation is neglected for forcings perturbations. The initial state for groundwater head was also perturbed using a Gaussian noise, with a null mean and standard deviation estimated from perturbed simulations (including hydraulic conductivity random perturbations to estimate the uncertainty of model state).

2.5.3 Evaluation of DA performance

The data assimilation (DA) scheme is evaluated by comparing the error evolution between the reference open loop simulation (OL, free run i.e. neither perturbations nor data assimilation applied) and a DA simulation. The error is assessed with the root mean squared error (RMSE), using the simulation and observation as reference (Eq. 11). As groundwater level are expressed as m a.s.l., RMSE is expressed in meters (m).

$$RMSE = \sqrt{\frac{1}{n}\sum_{i=1}^{n}(x_i - y_i^o)^2} \tag{11}$$

Where x_i is the simulated value and y_i^o is the observed equivalent, at the i-th timestep.

The improvement of DA over OL is measured by a Normalized Information Contribution (NIC, Eq. 12 ; e.g. Getirana et al. (2020); Hung et al. (2022))

$$NIC_{RMSE} = \frac{RMSE_{OL} - RMSE_{DA}}{RMSE_{OL}} \tag{12}$$

2.5.4 Simulation and DA settings

Data are assimilated, if available, with a 7 days cycle, corresponding to the model computation time step for groundwater head and river discharge. Two main experiments are conducted: (i) a short experiment (“srun”), with one and half year simulation

https://doi.org/10.5194/egusphere-2026-1504
Preprint. Discussion started: 18 May 2026

Table 1. Synthetic description of the seven experiments designed for data assimilation assessment

Experiment	Description	Evaluation
srun_gc_r100	Short experiment, loc. distance based, 100% of obs. assimilated	RMSE, NIC
srun_svg_r100	Short experiment, loc. correlation based, 100% of obs. assimilated	RMSE, NIC
srun_gc_r80	Short experiment, loc. distance based, 80% of obs. assimilated	RMSE, NIC
srun_svg_r80	Short experiment, loc. correlation based, 80% of obs. assimilated	RMSE, NIC
srun_gc_r50	Short experiment, loc. distance based, 50% of obs. assimilated	RMSE, NIC
srun_svg_r50	Short experiment, loc. correlation based, 50% of obs. assimilated	RMSE, NIC
srun_gc_r20	Short experiment, loc. distance based, 20% of obs. assimilated	RMSE, NIC
srun_svg_r20	Short experiment, loc. correlation based, 20% of obs. assimilated	RMSE, NIC
hrun	Hindcast from 2018 to 2024, DA and init forecast for each month	RMSE for different lead times

(from 2018-08 to 2020-02), composed by one year with data assimilation (DA) followed by six months of free run (no DA), as a seasonal forecast; (ii) a hindcast experiment ("hrun"), from 2018 to 2024, with at least 6 months of DA followed by six months of free run, repeated every month during the simulation time window to mimic the initialization of seasonal forecast at different times. For both experiments, the initial state (restart at 2018-08-01) is provided by the Aqui-FR 60 years reanalysis (Vergnes et al., 2020), thus avoiding the necessity for any spin-up time.

In order to verify the performance of DA, a validation experiment is conducted with the short experiment (*srun*). A set of X% of observation are randomly selected at the first cycle of assimilation, the remaining part is kept for validation purpose. This setup is repeated four times with different respectively 100, 80, 50, 20% of observation kept for assimilation. For each of these configurations, the assimilation is performed using the distance based Gaspari function ("gc"), and the variogram based method ("svg") as localization to compare performances on both assimilated and non assimilated observations. The NIC is computed as in Eq. 12.

For the *hrun* simulation (hindcast experiment), the RMSE is assessed at different forecast horizons (from 1 to 6 months) for every initialization dates. The RMSE is then averaged for each month (from 1 to 12) of initialization across the years included in the hindcast (2018-2024). For this experiment, all observations available are used (100% of observation sites), and data assimilation is performed using the correlation based localization method.

Table 1 sums up the different experiments conducted.

3 Results

3.1 Assessment of data assimilation performances

First, the DA performances is assessed with the *srun_gc_r80* and the *srun_svg_r80* experiments. The accumulated distribution of root-mean-square error (RMSE) on assimilated observation location shows impacts of data assimilation on error reduction

https://doi.org/10.5194/egusphere-2026-1504
Preprint. Discussion started: 18 May 2026

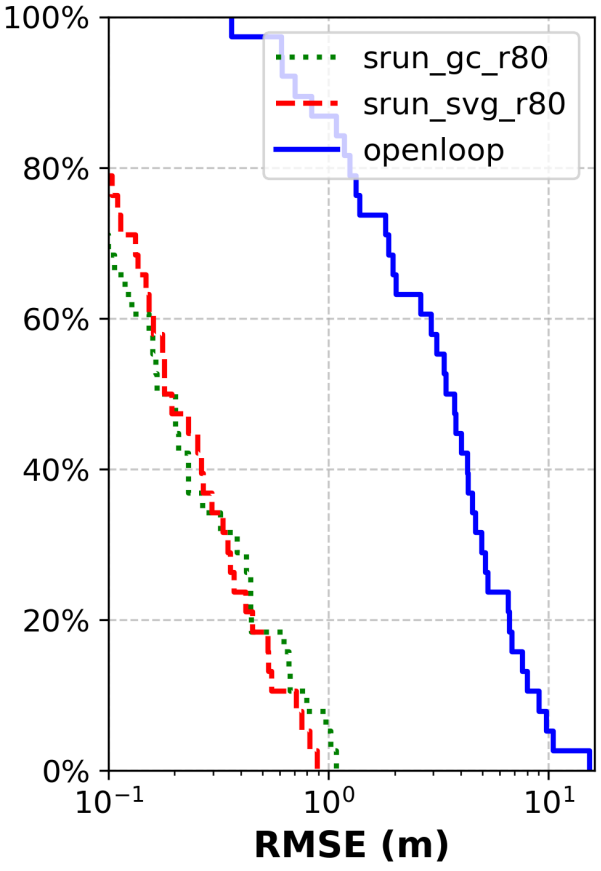

Figure 3. Root mean squared error (RMSE) distribution at observation sites for open-loop simulations and two data assimilation simulations using distance-based (gc) and variogram based (svg) localization methods.

Table 2. Summary of RMSE and NIC for data assimilation runs (with 80% of observations) and open-loop

Experiment	RMSE	NIC
open-loop	4.15	-
srun_gc_r80	0.30	0.92
srun_svg_r80	0.28	0.93

(Fig. 3). On average, the error is reduced by 92% between open loop simulation and DA simulation. Both localization methods show good performances at observation sites, with few differences on the RMSE computed, between the two experiments. The mean RMSE of the *srun_svg_r80* (0.28 m) is slightly lower than the error of the *srun_gc_r80* experiment (0.30 m) (Table 2).

https://doi.org/10.5194/egusphere-2026-1504
Preprint. Discussion started: 18 May 2026

Figure 4a to 4e show observed and simulated time series at different assimilated sites, which illustrate different behaviours of the model and DA performances, and Fig. 4f to 4h show time series at verification (non assimilated) sites. The comparison of simulated time series also show good performances for both localization methods at assimilated sites (Fig. 4).

For the first site (Fig. 4a), the assimilation shows a reduction in the bias and time lag of the simulation compared to observations. Distance based localization (*gc*) seems to produce slightly better results. After the forecast initialization, the persistence of the correction is low. After 3 to 4 months the DA and OL runs matches.

The second example site (Fig. 4b) show very good performances for DA for both localization method, with correlation based (*svg*) method showing lower error. Unlike the previous sites, initial error was essentially a positive bias (no dynamic/time discrepancy, $\mathbf{x}^b_{OL} > \mathbf{y}^o$). In consequence, during the six months of free run, the simulation remains very close to the observations. In other cases, forecast after DA can also lead to poorer results compared to open-loop (Fig. 4c), despite improvement on groundwater level estimation until last assimilation cycle.

In the fourth assimilated site (Fig. 4d), sequential DA also show good performances and is able to enhance simulations, compared to observations, with wrong initial dynamic in the open-loop. After the forecast initialization, mismatch between analysis and observation start to grow. Error is still lower than open-loop run after the six months of free run.

When comparing results for two closes cells, with one observation site assimilated (Fig. 4e) and one kept for verification (Fig. 4f), DA might lead to different results. These two piezometers are located in the east of the model domain, upstream, in an area influenced by withdrawals that are not well represented in the model. In both cases, the open-loop simulation reveals a smoother dynamic than the observations, showing more abrupt variations. The assimilated site show improvements over open-loop simulation, and better results with the *svg* localization method in the first part of the experiment. Despite being close, the two sites have different biases in the model (positive for the first one, negative for the second one), which lead to erroneous correction by DA. Nevertheless, groundwater dynamics seems correlated between the two sites, and the DA run is able to better capture the observed dynamic.

At verification sites, different behaviours are shown between the two localization methods used, with distanced based being better in some cases (e.g. Fig. 4g) or correlation based being slightly better (e.g. Fig. 4h).

3.2 Comparison with different density of observations

The validation experiment with different observation density (*srun_gc_rXX* and *srun_svg_rXX* experiments) show different performances between the two localization methods used. Figure 5 show the mean assimilation increment (for the *svg* method, i.e. correlation based) and the spatial distribution of NIC for different observation density and localization methods. Assimilated sites are represented as coloured dots and verification sites are represented as coloured squares.

DA increment, for example with the first experiment (*srun_svg_r100*), show that the absolute difference between assimilation and open-loop is greater or equal to 0.75 m at observation locations and is spread between dense observation areas, in both upstream and downstream directions, depending on the correlations found in the localization analysis. As observation sites are essentially located between the valleys, near the rivers, DA increment appears to be closed to zero. For 75% of assimilated

https://doi.org/10.5194/egusphere-2026-1504
Preprint. Discussion started: 18 May 2026

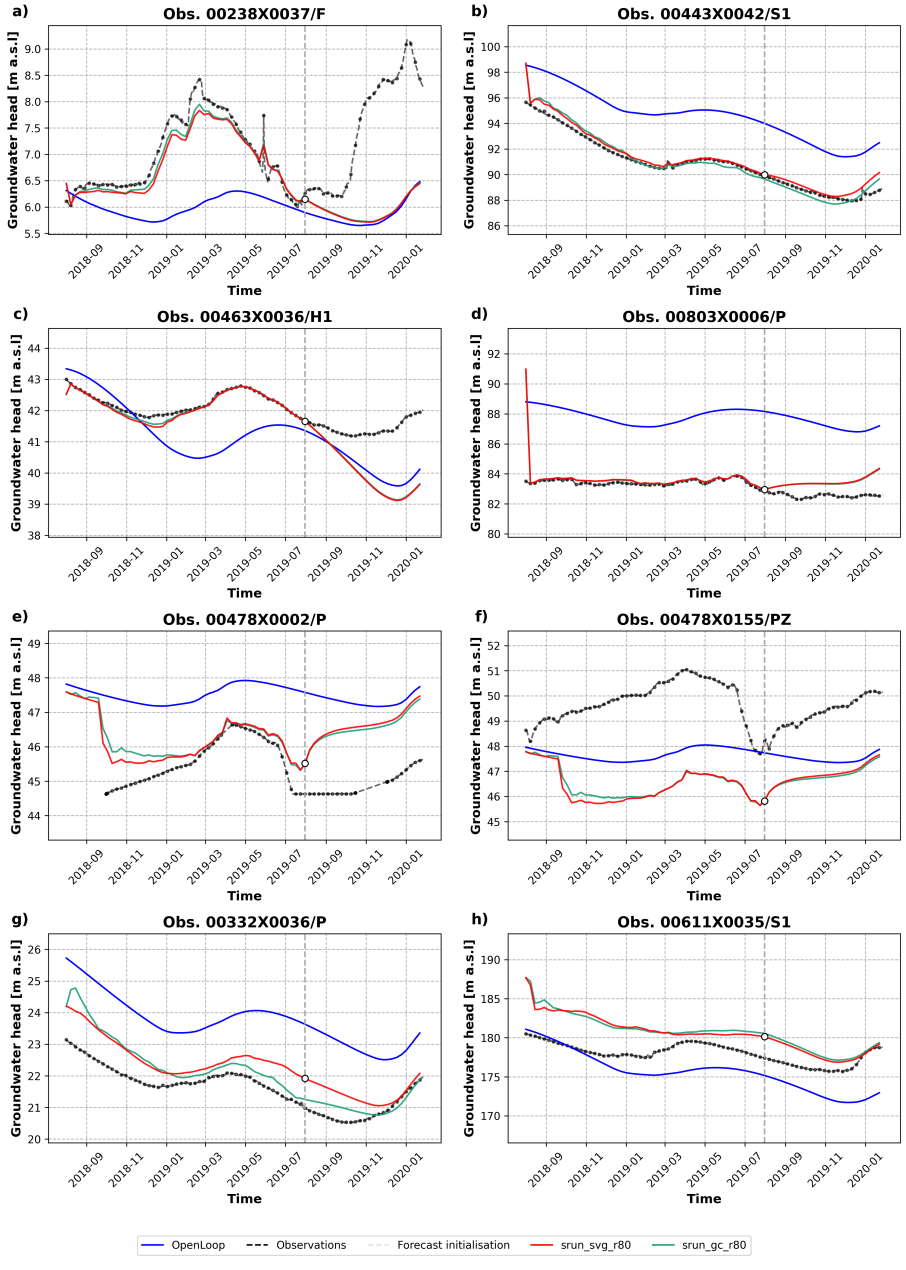

Figure 4. Time series of groundwater level at different observation sites. Panels (a) to (e) are for assimilated sites, panels (f) to (h) are for verification (non assimilated) sites. Black dots are observations, blue line is open-loop simulation, orange and green lines are DA simulation with distance based (gc) and correlation based (svg) localization methods respectively. Results are taken from the *srun_r80* (short run with assimilation of 80% of observations) experiment. Vertical dashed line indicate the initialization of the forecast (free run after DA is stopped). Observation sites are localized in Fig. 1 with their associated panel identifier.

https://doi.org/10.5194/egusphere-2026-1504
Preprint. Discussion started: 18 May 2026

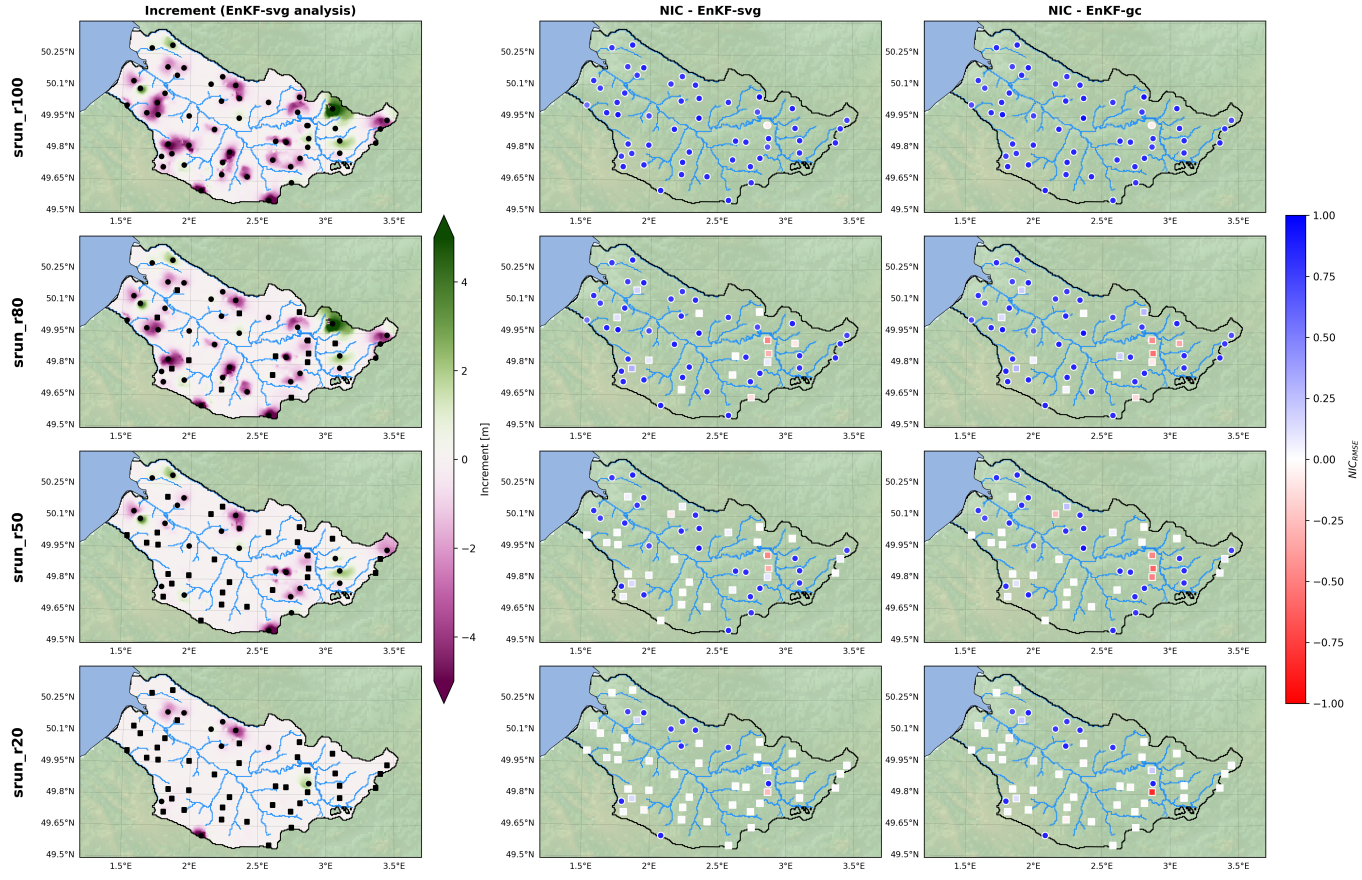

Figure 5. Spatial distribution of NIC for different observation densities and localization methods. The first column represents the DA increment (averaged for the experiment), the second column the NIC for correlation based localization (*svg*), the third column the NIC for distance based localization (*gc*). For the NIC columns, the blue values indicate an improvement of DA over open-loop simulation, while red values indicate a degradation. Coloured dots represent assimilated sites and coloured squares represent verification (non-assimilated) sites. The model's rivers are displayed as blue lines. The first row is for 100% of observations assimilated, the second row for 80%, the third row for 50%, and the fourth for 20%.

sites a NIC ≥ 0.85 is shown. Only two assimilation sites are not improved by the DA with either localization method. These are located in two neighbouring cells within the model domain.

With 80% of observation sites assimilated (experiment *srun_r80*), for both localization methods, the NIC is positive for all assimilated sites, indicating lower RMSE for the DA run than the open-loop run. For verification sites, similar results are obtained for both localization methods for all the assimilated sites. The correlation localization method (*svg*) show a mean NIC of +0.81 (max is +0.55 and min is +0.92), which indicate good average improvements over OL (RMSE reduction). For verification sites, computed NIC shows the same spatial patterns for both localization methods. Nevertheless, on two different sites distance based localization lead to better results (for example, in the northern part of sector "f" in Fig. 2 , for observation

https://doi.org/10.5194/egusphere-2026-1504
Preprint. Discussion started: 18 May 2026

00358X0216: NIC = +0.284 for *gc* and +0.002 for *svg*). Conversely, distance based localization also lead to bigger degradation of performance for different verification sites (e.g. near the "h" area in Fig. 2, observation site 00634X0147: NIC_{gc} = -0.558, NIC_{svg} = -0.312; observation site 00634X0039: NIC_{gc} = -0.092, NIC_{svg} = +0.092). In the south-west of the model grid, where different observation sites are close to each other, the reduction of assimilated observations (from 80 to 20%) lead to a reduction of DA improvement at the same verification sites for both localization methods. In this area, the DA increment shows different patterns based on the observations included.

For lower assimilated observation densities (50 and 20%), similar results are obtained, and distance based method tend to increase error on verification sites over the correlation based method. For both methods, when the assimilated observation density decrease the DA increment reach zero in most of the model domain.

3.3 Evaluation for forecasting

Results of the hindcast experiment are shown in Fig. 6 and Fig. 7. An example of hindcast time series is shown in Appendix (Fig. A2). During the 6-year simulation, on average for all observation sites, for each month of forecast initialization, the RMSE of the DA simulation is lower than that of the open-loop simulation during a seasonal forecast lead time (Fig. 6). The DA run RMSE is lower than 1 m at the initial step of the forecast and end to be greater or equal to 2 m after 6 months. OL run RMSE is varying between 3.5 and 4.5 m.

NIC distributions across the different observation sites (Fig. 7) indicates that at one month of lead time, 95% of the observation sites show a reduction of RMSE (NIC > 0) for every month of initialization, with only some outliers showing degradation of the error with the DA run. With the increase of the forecast range, NIC distributions are more widespread and the median value is lower (indicating more mitigated improvements). After a three months lead time, 75% of the NIC are still positives for every month of initialization, but more degradation (NIC < 0) and spatial heterogeneity (higher standard deviation) are also identified with these results.

Figure 8 shows an example of simulated groundwater level with DA at forecast initialization and at different forecast horizons (3 and 6 months) for the hindcast experiment (initialized for one month, here in April 2024). The assimilated groundwater level show significant differences with the open-loop, with a average absolute difference of 0.57 m (± 1.33 m) at initialization time. After 3 months of forecast, the mean absolute difference decrease to 0.49 m (± 1.22 m) and to 0.33 m (± 0.92 m) after 6 months. The impact of DA is still visible after 6 months of forecast, with some areas showing differences greater than 1 m compared to open-loop simulation. This spatial analysis allow identifying areas where the impact of DA fade quickly, with difference to open-loop spatially reduced after 3 months and close to zero after 6 months of forecasts.

4 Discussion

This paper presents the implementation of a data assimilation scheme, using a LEnKF algorithm, for groundwater level forecasting. We tested the method used with a regional hydrogeological model and different hindcast experiments, using real data

https://doi.org/10.5194/egusphere-2026-1504
Preprint. Discussion started: 18 May 2026

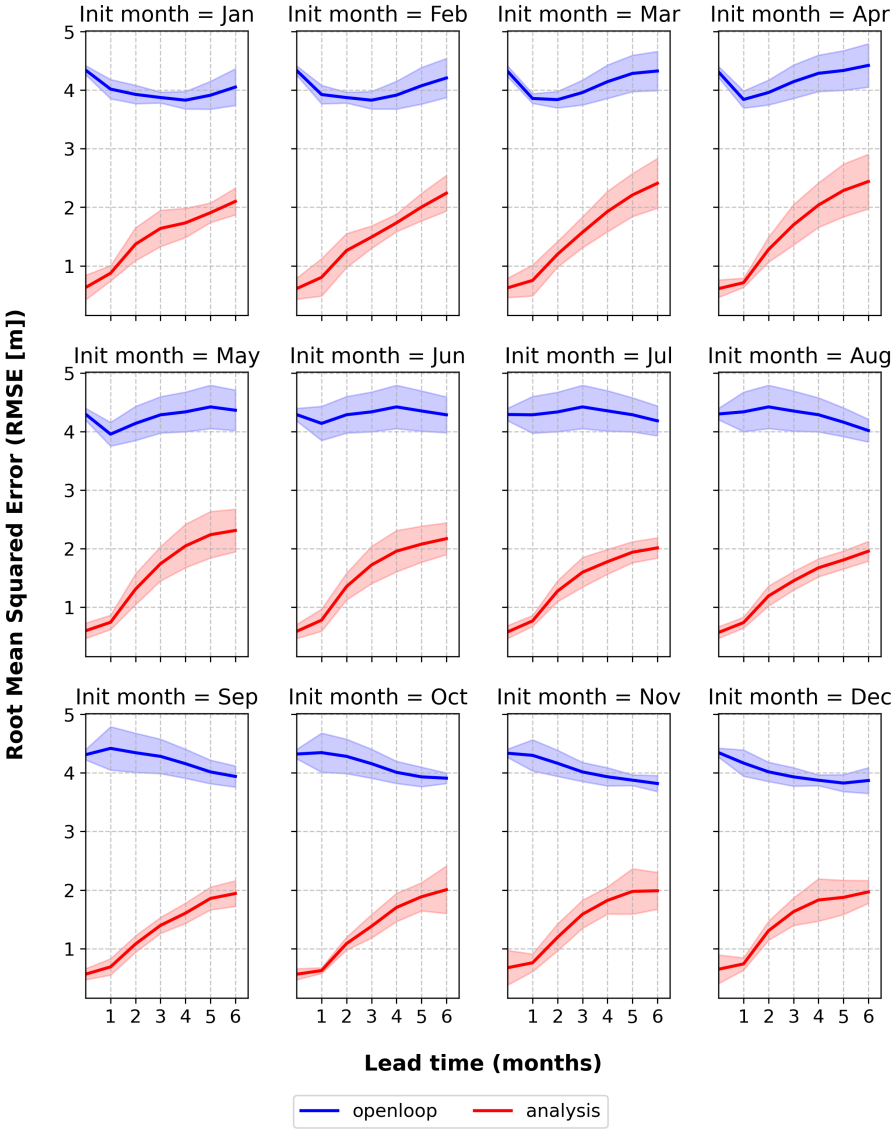

Figure 6. Evolution of the RMSE for the hindcast experiment. RMSE is averaged over all the observation sites and each month of the hindcast from 2018 to 2024. Each facet plot represents a different month of initialization for the forecast, from January to 12 December. X-axis indicates the lead time of the forecast, in months. The red line illustrates the RMSE for the hindcast experiment with assimilation, while the blue line represent the RMSE for the open-loop. Standard deviation across the hindcast years is represented by the shaded area.

and showing that groundwater level estimation can be improved and merged with data. The following section discusses the findings of this study.

https://doi.org/10.5194/egusphere-2026-1504
Preprint. Discussion started: 18 May 2026

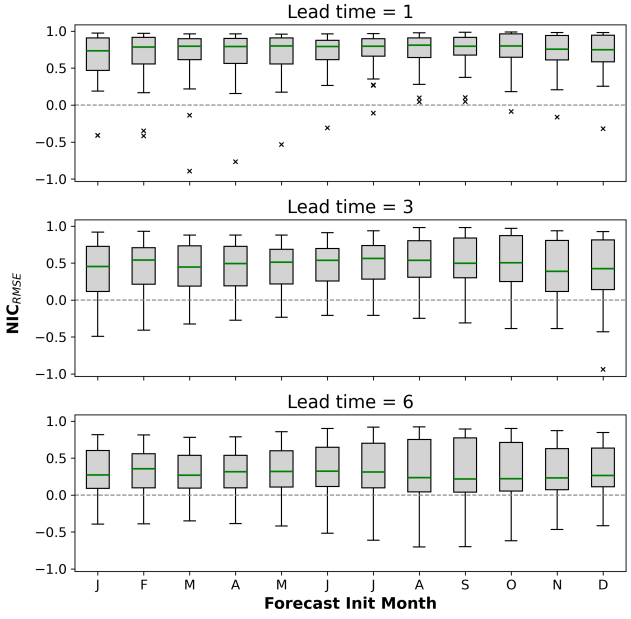

Figure 7. Distributions of NIC for the hindcast experiment at different forecast horizons ("lead times"; 1, 3 and 6 months) across all observations sites.

4.1 How does localization strategy impact results?

Two localization strategies have been used in this study: classical distance based localization and a correlation (semi-variance) based approach. For both methods, DA performed well and the estimation of groundwater level was improved for all the assimilated sites. At verification locations, some differences appear between the two methods. Distance based method was able to reduce the error at some observations sites where correlation method dampen too much DA increment, especially when verification site is located upstream of assimilated sites and correlation identified are too low. Because distance based method does not take into account any physical pattern, it is sometimes able to spread DA increment at longer distances, where no significant correlation are identified. Conversely, it also leads to stronger degradation of RMSE in other cases, even if observation and verification sites are relatively close to each other. In these cases, the correlation method appears to be more robust by identifying areas in the model domain that does not follow the same dynamic. These results are coherent with the conclusions of Li et al. (2023), who demonstrated that for real-world applications, DA improvement is sensitive to model structural errors and missing processes (e.g. human activities/withdrawals). As for piezometric statistical mapping, semi-variance allow capturing some physical pattern statistically. Unlike Revel et al. (2019), for groundwater state variable, we did not include any correction based on spatial direction (upstream/downstream) in the correlation calculation. This may explain some mitigated performances of the correlation based localization method. Thus, spatial correlation could be improved using anisotropic parameters for the semi-variogram analysis (Geiger et al., 2025). Besides, distance weighted computation within the correlation range, could be improved using another method than quasi-gaussian (GC) function. (e.g. using exponential decay, Verma et al.,

https://doi.org/10.5194/egusphere-2026-1504
Preprint. Discussion started: 18 May 2026

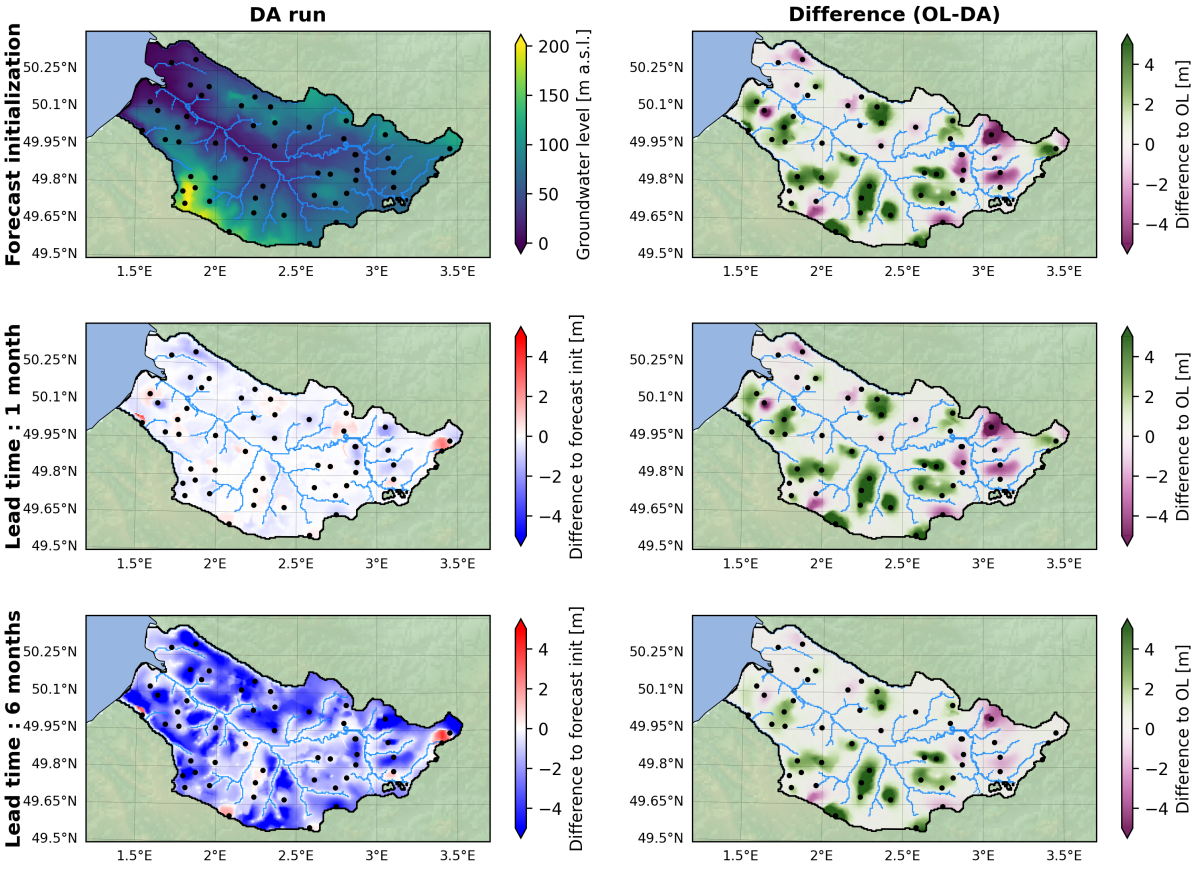

Figure 8. The simulated groundwater level with data assimilation at the initial forecast and the difference to this initial state at two different lead times is shown in column 1. Column 2 shows the difference with open-loop simulation for the hindcast experiment initialized in April 2024. The model's river network is shown as a blue line. The assimilated observation sites are represented as black dots.

2026). The semi-variance approach requires more preprocessing than the distance based method. One need to compute and fit a variogram model for every cell couple between observed cells and the rest of the model domain. For large domain with multiple observation sites this step can be computationally expensive (but only required once). Besides, if the distance based approach is simpler to use, it should be noted that to be efficient, this technique also needs to be calibrated, for example based on a variographic analysis as noted by Li et al. (2023). Although the semi-variogram approach can lead to more constraint spatial propagation of DA increment, the fact that degradation at verification sites is lower than distance based method is encouraging for applications with real data configurations (spatial/temporal observations sites density). Recently Vossepoel et al. (2025) also showed the advantage of correlation methods over distance based approach for oceanography reanalysis. The method used, as for other studies (Luo and Bhakta, 2020; Rasmussen et al., 2015), is based on ensemble correlation whereas our approach is based on open-loop spatio-temporal correlations. In future works, adaptive localization based on ensemble correlation, as

https://doi.org/10.5194/egusphere-2026-1504
Preprint. Discussion started: 18 May 2026

well as machine learning based algorithms (Cheng et al., 2023), could be tested for groundwater DA and compared to the semi-variance method.

In our case, the model represents a shallow aquifer with a slow dynamic. The spatial correlation of groundwater level is thus expected to be relatively high, and the semi-variogram method is able to capture this pattern. In other hydrogeological contexts, with more complex aquifer system and faster dynamic, the spatial correlation of groundwater level may be lower. In such cases, the correlation based localization may need to be adapted. Moreover, our model represents a single aquifer layer. In more complex multilayer aquifer system, the spatial correlation of groundwater level may be more complex to capture, especially with slow leakage between layers. Further investigations are needed to evaluate the performance of correlation based localization in such cases. Different methods could be tested to compute spatio-temporal correlation between all model states for multilayer aquifer systems, such as Empirical Orthogonal Functions (EOFs) analysis.

4.2 How does spatial observation density affect performances?

The different experiments with random selection of observations (80, 50 and 20%) show that the density of assimilated observations impact the DA performances. With fewer observations assimilated, the DA increment tends to be lower in most of the model domain, leading to fewer improvements at verification sites. A cumulative effect of multiple observations is seen with higher observation density, allowing a better propagation of DA increment in the model domain. Conversely, reducing the number of observations reduces the improvement. However, it does not deteriorate the results with the semi-variogram localization method.

At some point in the model space, when observation spatial density decrease, the DA increment is close to zero, regardless of the experiment. This is especially true in the valleys, near the rivers, where no observation sites are located. Correlation based localization lead to null increment in these areas, as estimated correlation in time series between valleys and plateaus are low. In general, we expect DA increment to be spread (upstream/downstream and as lateral flow) by the diffusion process of the groundwater flow equations. Hence, even we no direct influence of DA on a particular cell, a difference between OL and DA can be observed from a time step to another due to the physical diffusion. Here, the diffusion process is not visible from any observation sites to a valley downstream. This may be explained by the structural characteristics of the model and the boundary conditions used. The river network is represented as a Cauchy/Robin boundary condition, with a fixed head in the river. Thus, the river act as a strong sink/source for the aquifer, limiting the lateral propagation of DA increment near the rivers.

Besides, in our study, we did not use any specific observation operator. The simulated observation is an extraction of the simulation at the centre of the cell where is located the observation. The geometry of the model is smoothed by the domain resolution. Topography is average in cell, thus it does not share the same reference as observation. Hence, the observation error only includes sensor error and no representativeness error (representativeness of the observation in the model space). Still, we apply DA correction as if the reference altitude was the same for the state variable and the observation. By doing this, we did not take into account any specific configuration of the observation site. This could explain that for two adjacent cells, DA correction might be relevant for the dynamic but not for the bias, as seen in the time series. The development of an observation

https://doi.org/10.5194/egusphere-2026-1504
Preprint. Discussion started: 18 May 2026

operator could help to achieve better results, with a transformation function to get model equivalent of observations. Also, in real case applications, DA should include the most possible observations for a better analysis. Of course some may be filtered out, but more observations could possibly be assimilated, for example non-local observations or multiple observations in a same model cell. In such cases too, a relevant observation operator could improve DA configuration.

4.3 Is state assimilation efficient to improve groundwater level forecasting?

The hindcast evaluation of our DA scheme shows that groundwater level estimation can be improved over open-loop simulations, in a six months range forecast. As discussed in the previous sections, the initial calibration of the model, and the aquifer local dynamic may influence performances of the DA system. But these results are encouraging for the use of such workflow in hydrological seasonal forecasts.

The persistence of state data assimilation on groundwater forecast has been investigated in only a few studies, with varying lead times. He et al. (2019) used a similar hydrological model with DA experiments and investigated the forecast accuracy with a 48 hours lead time. Hendricks Franssen et al. (2011) demonstrated a positive effect of DA on a hydrological model's predictions, up to 10 days after the update with state DA (and more with a synthetic case). Getirana et al. (2020) showed benefits of DA during a seasonal forecast range, using a land surface model and ensemble forecast as forcings. Their results where contrasted based on the location (and human influenced or local hydrogeological processes). In this study, we tested DA effect on a forecast with six months range, showing the average error was still lower than open-loop simulations.

These results, of course, depend on the dynamics of the aquifer. Here, the modelled chalk aquifer shows multiannual and seasonal cycles (Baulon et al., 2022). This inertia leads to a greater persistence of DA corrections than in hydrosystems with quicker fluctuations in water levels. In some areas of the Somme model where the groundwater level has a shorter response time to forcing, the DA's performance is less good. For such configurations, dual state-parameters or two-steps DA may be required if initial parameters do not lead to an accurate reproduction of groundwater levels, in order to improve reanalysis or seasonal forecasts. Nevertheless, this approach remains relevant for our application in northern France, where most piezometers show a predominance of multiannual cycles (Baulon et al., 2022). Still, even in such cases, the model calibration remains a key step to ensure good performances of DA. Here, we chose to only update state as a first step, as the calibration of hydraulic parameters is the results of expertise on the model and evolutions since its first version (Amraoui et al., 2002). But if the model is unable to accurately simulate the main dynamics of the aquifer, DA may not be able to correct it properly. Several authors have also shown the benefits of dual state parameters for groundwater estimations (e.g., Hendricks Franssen et al., 2011; Rasmussen et al., 2015; Hung et al., 2022). Therefore, a two steps DA, with a first step of parameter update followed by a state update, could be more efficient in such cases. This method will be explored in our future works.

As shown in Fig. 4, open-loop time series might be affected by bias or time lag compared to observations. If commons groundwater parameter (hydraulic conductivity and storage/specific yield) updates with DA might help, one must also bear in mind the conceptual model. In our case, the time lag in the modelled dynamics could be due to the complex response of the aquifer to forcings and UZ processes being represented inaccurately. (Habets et al., 2010; Thiéry et al., 2018). In the model chosen for this research, the UZ representation was simplified with a LSM coupled to a conceptual approach as transfer

https://doi.org/10.5194/egusphere-2026-1504
Preprint. Discussion started: 18 May 2026

function to the groundwater layer, used as explained in section 2. In comparison, different studies used an explicit representation of unsaturated flows with DA (e.g., Hung et al., 2022; Li et al., 2023). Computation burden of such model is extremely higher than computing groundwater level (GWL) using a layered saturated model, but a better representation of vertical fluxes through unsaturated flow might be required to improve this part (Thiéry et al., 2018).

In this study, we assimilated groundwater head measurements to improve the simulated GWL with DA updates. Actually, in the Aqui-FR modelling platform, drought seasonal forecasts are performed using a transformation of simulated GWL, with a Standardized Piezometric Level Index (Vergnes et al., 2020) representing a form of GWL anomaly. As discussed previously, DA is able to correct the model state for biases and wrong dynamics with sequential updates, but persistence may vary because of intrinsic characteristics of the aquifer, initial parameters set, and/or wrong representation of the measurements in the model space. The GWL anomaly computed after DA run may also be impacted either because of a shift induced by DA updates or because of the slow return to OL state. Hence, this behaviour might impact the identification of drought and can still lead to performances when computing GWL anomaly or standardized index. To overcome this, it may be useful in future works to assimilate GWL anomalies instead of absolute measurements, through the observation operator for example.

Finally, in this study, we only used atmospheric and land surface reanalysis as forcings during the hindcast experiment. Studies show the benefits of DA for river discharge forecasting with sequential assimilation method and in situ observations, for example in France (Thirel et al., 2010) or in Sweden (Musuuza et al., 2023). Improvements are also expected for groundwater seasonal forecast (Getirana et al., 2020). For a better evaluation of DA impact on groundwater forecasts, our future works should also use ensemble seasonal forecasts forcings.

5 Conclusions

This study investigated the implementation of a data assimilation scheme using a Local Ensemble Kalman Filter algorithm for groundwater level forecasting. The method was tested with a regional hydrogeological model of the Somme basin (France) and real piezometric data, within the Aqui-FR hydrometeorological modelling platform.

Two localization methods were tested: a classical distance based approach and a correlation based approach, using semi-variogram analysis of the model domain and open-loop simulations. Both methods showed good performances at assimilated sites, with a reduction of RMSE greater than 90% compared to open-loop simulation. At verification sites, correlation based localization showed more robust results, with less degradation of RMSE compared to distance based method. The correlation based method was able to capture physical patterns of groundwater level dynamic, leading to a better identification of areas in the model domain that do not share the same dynamic. In the future, the correlation computation could be improved by including anisotropic parameters in the semi-variogram analysis or multilayer case study.

The potential of the DA scheme for seasonal forecasting was evaluated through a hindcast experiment. Results showed that groundwater level estimation can be improved over open-loop simulation, up to a 6 months lead time. These results are encouraging for the use of such workflow in hydrological seasonal forecasts, especially in hydrogeological contexts with slow dynamics. Future work will include an assessment of ensemble seasonal forecasts for groundwater level forecasting.

https://doi.org/10.5194/egusphere-2026-1504
Preprint. Discussion started: 18 May 2026

Appendix A: Supplementary figures

A1 Observed and simulated time series and frequency

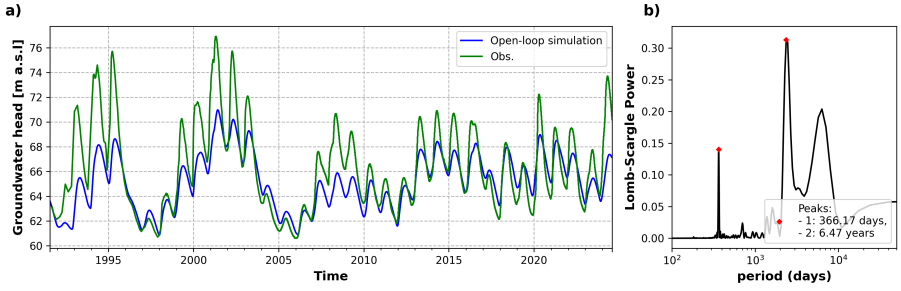

Figure A1. Example of (a) typical time series of simulated (open-loop) and observed groundwater level in the study area and (b) associated spectral analysis, showing annual and multiannual cycle pattern. Spectral analysis was computed using a Lomb-Scargle periodogram (Scargle, 1982).

A2 Hindcast time serie

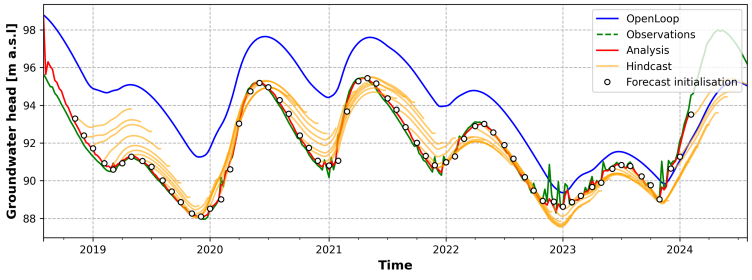

Figure A2. Example time series showing open-loop simulation (blue line) against analysis (red line), hindcast simulations (orange) and observations (green). White dots indicate every forecast initialization. Time series during each forecast are shown as orange lines. The observation sites correspond to the Fig. 4b, also located in Fig. 2

https://doi.org/10.5194/egusphere-2026-1504
Preprint. Discussion started: 18 May 2026

Code and data availability. The groundwater level data used are available in the French national database ADES (https://ades.eaufrance.fr/, Winckel et al. (2022), last access: 10 July 2025). The SAFRAN/ISBA reanalysis is available at https://meteo.data.gouv.fr/. As part of the AquiFR project led by the OFB ("Office Français pour la Biodiversité" in French for French Office for Biodiversity), the AquiFR modelling platform is not directly hosted on any public repository. Details about the Aqui-FR code can be gathered upon e-mail request to simon.munier@meteo.fr. Questions about the MARTHE code can be requested to marthe@brgm.fr. The data assimilation code is available at https://doi.org/10.5281/zenodo.18953669. All data and code necessary to reproduce the figures from this study are available from the following Zenodo repository: https://doi.org/10.5281/zenodo.18851277.

Author contributions. AM, JPV, SM and FH conceptually designed the work. AM developed the assimilation code. SM, JPV and FH developed and maintain the Aqui-FR code that is used to add assimilation. AM conducted the simulations and analyses and wrote the first draft of the paper. All authors revised the paper and contributed to the analysis and discussion.

Competing interests. The contact author has declared that none of the authors has any competing interests.

Acknowledgements. This work benefited from State fundings managed by the Agence Nationale de la Recherche (ANR) under the France 2030 programme, reference ANR-22-PEXO-0003, as part of the OneWater - Eau Bien Commun national research programme. The authors acknowledge BRGM for providing SAPHIR computing and storage resources, and Faïza Boulahya for her help. The authors would also like to express their gratitude to the open-source community on which this work is based, especially the developers of NumPy (Harris et al., 2020), SciPy (Virtanen et al., 2020) and Matplotlib (Hunter, 2007). Finally, the authors would like to thank all the contributors to the Aqui-FR project.

https://doi.org/10.5194/egusphere-2026-1504
Preprint. Discussion started: 18 May 2026

References

Albergel, C., Dutra, E., Bonan, B., Zheng, Y., Munier, S., Balsamo, G., de Rosnay, P., Muñoz-Sabater, J., and Calvet, J.-C.: Monitoring and Forecasting the Impact of the 2018 Summer Heatwave on Vegetation, Remote Sensing, 11, 520, https://doi.org/10.3390/rs11050520, 2019.

Alzraiee, A. H., White, J. T., Knowling, M. J., Hunt, R. J., and Fienen, M. N.: A Scalable Model-Independent Iterative Data Assimilation Tool for Sequential and Batch Estimation of High Dimensional Model Parameters and States, Environmental Modelling & Software, 150, 105 284, https://doi.org/10.1016/j.envsoft.2021.105284, 2022.

Amraoui, N., Golaz, C., Mardhel, V., Négrel, P., Petit, V., Pinault, J., and Pointet, T.: Simulation par modèle des hautes eaux de la Somme., Tech. Rep. BRGM/RP-51827-FR, BRGM, Orléans, http://ficheinfoterre.brgm.fr/document/RP-51827-FR, 2002.

Anderson, J. L.: An Ensemble Adjustment Kalman Filter for Data Assimilation, Monthly Weather Review, 129, 2884–2903, https://doi.org/10.1175/1520-0493(2001)129<2884:AEAKFF>2.0.CO;2, 2001.

Anderson, J. L.: An Adaptive Covariance Inflation Error Correction Algorithm for Ensemble Filters, Tellus A: Dynamic Meteorology and Oceanography, 59, 210–224, https://doi.org/10.1111/j.1600-0870.2006.00216.x, 2007.

Baulon, L., Massei, N., Allier, D., Fournier, M., and Bessiere, H.: Influence of Low-Frequency Variability on High and Low Groundwater Levels: Example of Aquifers in the Paris Basin, Hydrology and Earth System Sciences, 26, 2829–2854, https://doi.org/10.5194/hess-26-2829-2022, 2022.

Baulon, L., Massei, N., Dieppois, B., Fossa, M., Allier, D., Bessière, H., and Fournier, M.: Large-Scale Climate Drivers of Groundwater Level Variations in Northern France over the Last Century, Journal of Hydrology, 656, 132 937, https://doi.org/10.1016/j.jhydrol.2025.132937, 2025.

Belleflamme, A., Goergen, K., Wagner, N., Kollet, S., Bathiany, S., El Zohbi, J., Rechid, D., Vanderborght, J., and Vereecken, H.: Hydrological Forecasting at Impact Scale: The Integrated ParFlow Hydrological Model at 0.6 Km for Climate Resilient Water Resource Management over Germany, Frontiers in Water, 5, https://www.frontiersin.org/articles/10.3389/frwa.2023.1183642, 2023.

Biella, R., Shyrokaya, A., Ionita, M., Vignola, R., Sutanto, S., Todorovic, A., Teutschbein, C., Cid, D., Llasat, M. C., Alencar, P., Matanó, A., Ridolfi, E., Moccia, B., Pechlivanidis, I., van Loon, A., Wendt, D., Stenfors, E., Russo, F., Vidal, J.-P., Barker, L., de Brito, M. M., Lam, M., Bláhová, M., Trambauer, P., Hamed, R., McGrane, S. J., Ceola, S., Bakke, S. J., Krakovska, S., Nagavciuc, V., Tootoonchi, F., Di Baldassarre, G., Hauswirth, S., Maskey, S., Zubkovych, S., Wens, M., and Tallaksen, L. M.: The 2022 Drought Needs to Be a Turning Point for European Drought Risk Management, Egusphere, https://doi.org/10.5194/egusphere-2024-2069, 2024.

Boo, K. B. W., El-Shafie, A., Othman, F., Khan, M. M. H., Birima, A. H., and Ahmed, A. N.: Groundwater Level Forecasting with Machine Learning Models: A Review, Water Research, 252, 121 249, https://doi.org/10.1016/j.watres.2024.121249, 2024.

Botto, A., Belluco, E., and Camporese, M.: Multi-Source Data Assimilation for Physically Based Hydrological Modeling of an Experimental Hillslope, Hydrology and Earth System Sciences, 22, 4251–4266, https://doi.org/10.5194/hess-22-4251-2018, 2018.

Burgers, G., van Leeuwen, P. J., and Evensen, G.: Analysis Scheme in the Ensemble Kalman Filter, Monthly Weather Review, 126, 1719–1724, https://doi.org/10.1175/1520-0493(1998)126<1719:ASITEK>2.0.CO;2, 1998.

Camporese, M. and Girotto, M.: Recent Advances and Opportunities in Data Assimilation for Physics-Based Hydrological Modeling, Frontiers in Water, 4, https://doi.org/10.3389/frwa.2022.948832, 2022.

Camporese, M., Paniconi, C., Putti, M., and Salandin, P.: Ensemble Kalman Filter Data Assimilation for a Process-Based Catchment Scale Model of Surface and Subsurface Flow, Water Resources Research, 45, W10 421, https://doi.org/10.1029/2008WR007031, 2009.

https://doi.org/10.5194/egusphere-2026-1504
Preprint. Discussion started: 18 May 2026

Carrassi, A., Bocquet, M., Bertino, L., and Evensen, G.: Data Assimilation in the Geosciences: An Overview of Methods, Issues, and Perspectives, WIREs Climate Change, 9, e535, https://doi.org/10.1002/wcc.535, 2018.

Cheng, S., Quilodrán-Casas, C., Ouala, S., Farchi, A., Liu, C., Tandeo, P., Fablet, R., Lucor, D., Iooss, B., Brajard, J., Xiao, D., Janjic, T., Ding, W., Guo, Y., Carrassi, A., Bocquet, M., and Arcucci, R.: Machine Learning With Data Assimilation and Uncertainty Quantification for Dynamical Systems: A Review, IEEE/CAA Journal of Automatica Sinica, 10, 1361–1387, https://doi.org/10.1109/JAS.2023.123537, 2023.

Clark, M. P., Rupp, D. E., Woods, R. A., Zheng, X., Ibbitt, R. P., Slater, A. G., Schmidt, J., and Uddstrom, M. J.: Hydrological Data Assimilation with the Ensemble Kalman Filter: Use of Streamflow Observations to Update States in a Distributed Hydrological Model, Advances in Water Resources, 31, 1309–1324, https://doi.org/10.1016/j.advwatres.2008.06.005, 2008.

Dasgupta, A., Arnal, L., Emerton, R., Harrigan, S., Matthews, G., Muhammad, A., O'Regan, K., Pérez-Ciria, T., Valdez, E., van Osnabrugge, B., Werner, M., Buontempo, C., Cloke, H., Pappenberger, F., Pechlivanidis, I. G., Prudhomme, C., Ramos, M.-H., and Salamon, P.: Connecting Hydrological Modelling and Forecasting from Global to Local Scales: Perspectives from an International Joint Virtual Workshop, Journal of Flood Risk Management, n/a, e12 880, https://doi.org/10.1111/jfr3.12880, 2022.

de Marsily, G.: Quantitative Hydrogeology: Groundwater Hydrology for Engineers, Acad. Press, San Diego, 5. [print.] edn., ISBN 978-0-12-208916-4 978-0-12-208915-2, https://gw-project.org/books/quantitative-hydrogeology-groundwater-hydrology-for-engineers/, 1986.

de Marsily, G., Delhomme, J. P., Coudrain-Ribstein, A., and Lavenue, A. M.: Four Decades of Inverse Problems in Hydrogeology, in: Theory, Modeling, and Field Investigation in Hydrogeology: A Special Volume in Honor of Shlomo P. Neumans 60th Birthday, edited by Zhang, D. and Winter, C. L., p. 0, Geological Society of America, ISBN 978-0-8137-2348-8, https://doi.org/10.1130/0-8137-2348-5.1, 2000.

Doherty, J. and Moore, C.: Decision Support Modeling: Data Assimilation, Uncertainty Quantification, and Strategic Abstraction, Groundwater, 58, 327–337, https://doi.org/10.1111/gwat.12969, 2020.

Ehrendorfer, M.: A Review of Issues in Ensemble-Based Kalman Filtering, Meteorologische Zeitschrift (Berlin), 16, https://doi.org/10.1127/0941-2948/2007/0256, 2007.

Evensen, G.: Sequential Data Assimilation with a Nonlinear Quasi-Geostrophic Model Using Monte Carlo Methods to Forecast Error Statistics, Journal of Geophysical Research: Oceans, 99, 10 143–10 162, https://doi.org/10.1029/94JC00572, 1994.

Evensen, G.: The Ensemble Kalman Filter: Theoretical Formulation and Practical Implementation, Ocean Dynamics, 53, 343–367, https://doi.org/10.1007/s10236-003-0036-9, 2003.

Farr, T. G., Rosen, P. A., Caro, E., Crippen, R., Duren, R., Hensley, S., Kobrick, M., Paller, M., Rodriguez, E., Roth, L., Seal, D., Shaffer, S., Shimada, J., Umland, J., Werner, M., Oskin, M., Burbank, D., and Alsdorf, D.: The Shuttle Radar Topography Mission, Reviews of Geophysics, 45, https://doi.org/10.1029/2005RG000183, 2007.

Gaspari, G. and Cohn, S. E.: Construction of Correlation Functions in Two and Three Dimensions, Quarterly Journal of the Royal Meteorological Society, 125, 723–757, https://doi.org/10.1002/qj.49712555417, 1999.

Geiger, J., Finkel, M., and Cirpka, O. A.: Estimating the Full Anisotropy of the Covariance Function in Geostatistical Inversion Using the Pilot-Point Ensemble Kalman Filter, Advances in Water Resources, 206, 105 103, https://doi.org/10.1016/j.advwatres.2025.105103, 2025.

Getirana, A., Rodell, M., Kumar, S., Beaudoing, H. K., Arsenault, K., Zaitchik, B., Save, H., and Bettadpur, S.: GRACE Improves Seasonal Groundwater Forecast Initialization over the United States, Journal of Hydrometeorology, 21, 59–71, https://doi.org/10.1175/JHM-D-19-0096.1, 2020.

https://doi.org/10.5194/egusphere-2026-1504
Preprint. Discussion started: 18 May 2026

Guardiola-Albert, C., Naranjo-Fernández, N., Rivera-Rivera, J. S., Gómez Fontalva, J. M., Aguilera, H., Ruiz-Bermudo, F., and Rodríguez-Rodríguez, M.: Enhancing Groundwater Management with GRACE-based Groundwater Estimates from GLDAS-2.2: A Case Study of the Almonte-Marismas Aquifer, Spain, Hydrogeology Journal, https://doi.org/10.1007/s10040-024-02838-3, 2024.

Guillaumot, L., Munier, S., Abhervé, R., Vergnes, J.-P., Jeantet, A., Le Moigne, P., and Habets, F.: Are Regional Groundwater Models Suitable for Simulating Wetlands, Rivers and Intermittence? The Example of the French AquiFR Platform, Journal of Hydrology, 644, 132 019, https://doi.org/10.1016/j.jhydrol.2024.132019, 2024.

Habets, F., Gascoin, S., Korkmaz, S., Thiéry, D., Zribi, M., Amraoui, N., Carli, M., Ducharne, A., Leblois, E., Ledoux, E., Martin, E., Noilhan, J., Ottlé, C., and Viennot, P.: Multi-Model Comparison of a Major Flood in the Groundwater-Fed Basin of the Somme River (France), Hydrology and Earth System Sciences, 14, 99–117, https://doi.org/10.5194/hess-14-99-2010, 2010.

Hamill, T. M., Whitaker, J. S., and Snyder, C.: Distance-Dependent Filtering of Background Error Covariance Estimates in an Ensemble Kalman Filter, Monthly Weather Review, 129, 2776–2790, https://doi.org/10.1175/1520-0493(2001)129<2776:DDFOBE>2.0.CO;2, 2001.

Harris, C. R., Millman, K. J., van der Walt, S. J., Gommers, R., Virtanen, P., Cournapeau, D., Wieser, E., Taylor, J., Berg, S., Smith, N. J., Kern, R., Picus, M., Hoyer, S., van Kerkwijk, M. H., Brett, M., Haldane, A., del Río, J. F., Wiebe, M., Peterson, P., Gérard-Marchant, P., Sheppard, K., Reddy, T., Weckesser, W., Abbasi, H., Gohlke, C., and Oliphant, T. E.: Array Programming with NumPy, Nature, 585, 357–362, https://doi.org/10.1038/s41586-020-2649-2, 2020.

He, X., Lucatero, D., Ridler, M.-E., Madsen, H., Kidmose, J., Hole, Ø., Petersen, C., Zheng, C., and Refsgaard, J. C.: Real-Time Simulation of Surface Water and Groundwater with Data Assimilation, Advances in Water Resources, 127, 13–25, https://doi.org/10.1016/j.advwatres.2019.03.004, 2019.

Hendricks Franssen, H. J. and Kinzelbach, W.: Real-Time Groundwater Flow Modeling with the Ensemble Kalman Filter: Joint Estimation of States and Parameters and the Filter Inbreeding Problem, Water Resources Research, 44, https://doi.org/10.1029/2007WR006505, 2008.

Hendricks Franssen, H. J. and Kinzelbach, W.: Ensemble Kalman Filtering versus Sequential Self-Calibration for Inverse Modelling of Dynamic Groundwater Flow Systems, Journal of Hydrology, 365, 261–274, https://doi.org/10.1016/j.jhydrol.2008.11.033, 2009.

Hendricks Franssen, H. J., Kaiser, H. P., Kuhlmann, U., Bauser, G., Stauffer, F., Müller, R., and Kinzelbach, W.: Operational Real-Time Modeling with Ensemble Kalman Filter of Variably Saturated Subsurface Flow Including Stream-Aquifer Interaction and Parameter Updating, Water Resources Research, 47, W02 532, https://doi.org/10.1029/2010WR009480, 2011.

Houborg, R., Rodell, M., Li, B., Reichle, R., and Zaitchik, B. F.: Drought Indicators Based on Model-Assimilated Gravity Recovery and Climate Experiment (GRACE) Terrestrial Water Storage Observations, Water Resources Research, 48, https://doi.org/10.1029/2011WR011291, 2012.

Houtekamer, P. L. and Mitchell, H. L.: A Sequential Ensemble Kalman Filter for Atmospheric Data Assimilation, Monthly Weather Review, 129, 123–137, https://doi.org/10.1175/1520-0493(2001)129<0123:ASEKFF>2.0.CO;2, 2001.

Hung, C. P., Schalge, B., Baroni, G., Vereecken, H., and Hendricks Franssen, H.-J.: Assimilation of Groundwater Level and Soil Moisture Data in an Integrated Land Surface-Subsurface Model for Southwestern Germany, Water Resources Research, 58, e2021WR031 549, https://doi.org/10.1029/2021WR031549, 2022.

Hunter, J. D.: Matplotlib: A 2D Graphics Environment, Computing in Science & Engineering, 9, 90–95, https://doi.org/10.1109/MCSE.2007.55, 2007.

Jeantet, A., Vergnes, J.-P., Munier, S., and Habets, F.: Climate Change Impacts on Groundwater Simulated Using the AquiFR Modelling Platform, EGUsphere, pp. 1–44, https://doi.org/10.5194/egusphere-2025-93, 2025.

https://doi.org/10.5194/egusphere-2026-1504
Preprint. Discussion started: 18 May 2026

Kurtz, W., He, G., Kollet, S. J., Maxwell, R. M., Vereecken, H., and Hendricks Franssen, H.-J.: TerrSysMP–PDAF (Version 1.0): A Modular High-Performance Data Assimilation Framework for an Integrated Land Surface–Subsurface Model, Geoscientific Model Development, 9, 1341–1360, https://doi.org/10.5194/gmd-9-1341-2016, 2016.

Le Moigne, P., Besson, F., Martin, E., Boé, J., Boone, A., Decharme, B., Etchevers, P., Faroux, S., Habets, F., Lafaysse, M., Leroux, D., and Rousset-Regimbeau, F.: The Latest Improvements with SURFEX v8.0 of the Safran–Isba–Modcou Hydrometeorological Model for France, Geoscientific Model Development, 13, 3925–3946, https://doi.org/10.5194/gmd-13-3925-2020, 2020.

Leroux, D., Munier, S., Habets, F., Besson, F., Regimbeau, F. R., Moigne, P. L., Vergnes, J.-P., Viennot, P., Etchevers, P., and Amraoui, N.: Seasonal Forecast of the Groundwater Resource in France, in: European Meteorological Society Annual Meeting, p. 33, Copenhagen, Denmark, https://hal-mines-paristech.archives-ouvertes.fr/hal-02383889, 2019.

Li, F., Kurtz, W., Hung, C. P., Vereecken, H., and Hendricks Franssen, H.-J.: Water Table Depth Assimilation in Integrated Terrestrial System Models at the Larger Catchment Scale, Frontiers in Water, 5, https://www.frontiersin.org/journals/water/articles/10.3389/frwa.2023.1150999, 2023.

Li, H., Luo, L., Wood, E. F., and Schaake, J.: The Role of Initial Conditions and Forcing Uncertainties in Seasonal Hydrologic Forecasting, Journal of Geophysical Research: Atmospheres, 114, https://doi.org/10.1029/2008JD010969, 2009.

Luo, X. and Bhakta, T.: Automatic and Adaptive Localization for Ensemble-Based History Matching, Journal of Petroleum Science and Engineering, 184, 106 559, https://doi.org/10.1016/j.petrol.2019.106559, 2020.

Mackay, J. D., Jackson, C. R., Brookshaw, A., Scaife, A. A., Cook, J., and Ward, R. S.: Seasonal Forecasting of Groundwater Levels in Principal Aquifers of the United Kingdom, Journal of Hydrology, 530, 815–828, https://doi.org/10.1016/j.jhydrol.2015.10.018, 2015.

Manlay, A.: Aqui-DA: A Data Assimilation Library for the Aqui-FR Hydrometeorological Modelling Platform, Zenodo, https://doi.org/10.5281/zenodo.18953669, 2026.

Maréchal, J.-C. and Rouillard, J.: Groundwater in France: Resources, Use and Management Issues, in: Sustainable Groundwater Management: A Comparative Analysis of French and Australian Policies and Implications to Other Countries, edited by Rinaudo, J.-D., Holley, C., Barnett, S., and Montginoul, M., Global Issues in Water Policy, pp. 17–45, Springer International Publishing, Cham, ISBN 978-3-030-32766-8, https://doi.org/10.1007/978-3-030-32766-8_2, 2020.

Masson, V., Le Moigne, P., Martin, E., Faroux, S., Alias, A., Alkama, R., Belamari, S., Barbu, A., Boone, A., Bouyssel, F., Brousseau, P., Brun, E., Calvet, J.-C., Carrer, D., Decharme, B., Delire, C., Donier, S., Essaouini, K., Gibelin, A.-L., Giordani, H., Habets, F., Jidane, M., Kerdraon, G., Kourzeneva, E., Lafaysse, M., Lafont, S., Lebeaupin Brossier, C., Lemonsu, A., Mahfouf, J.-F., Marguinaud, P., Mokhtari, M., Morin, S., Pigeon, G., Salgado, R., Seity, Y., Taillefer, F., Tanguy, G., Tulet, P., Vincendon, B., Vionnet, V., and Voldoire, A.: The SURFEXv7.2 Land and Ocean Surface Platform for Coupled or Offline Simulation of Earth Surface Variables and Fluxes, Geoscientific Model Development, 6, 929–960, https://doi.org/10.5194/gmd-6-929-2013, 2013.

Morzfeld, M. and Hodyss, D.: A Theory for Why Even Simple Covariance Localization Is So Useful in Ensemble Data Assimilation, Monthly Weather Review, 151, 717–736, https://doi.org/10.1175/MWR-D-22-0255.1, 2023.

Musuuza, J. L., Crochemore, L., and Pechlivanidis, I. G.: Evaluation of Earth Observations and in Situ Data Assimilation for Seasonal Hydrological Forecasting, Water Resources Research, 59, https://doi.org/10.1029/2022WR033655, 2023.

Pascal, C., Ferrant, S., Selles, A., Maréchal, J.-C., Paswan, A., and Merlin, O.: Evaluating Downscaling Methods of GRACE (Gravity Recovery and Climate Experiment) Data: A Case Study over a Fractured Crystalline Aquifer in Southern India, Hydrology and Earth System Sciences, 26, 4169–4186, https://doi.org/10.5194/hess-26-4169-2022, 2022.

https://doi.org/10.5194/egusphere-2026-1504
Preprint. Discussion started: 18 May 2026

Piazzi, G., Thirel, G., Perrin, C., and Delaigue, O.: Sequential Data Assimilation for Streamflow Forecasting: Assessing the Sensitivity to Uncertainties and Updated Variables of a Conceptual Hydrological Model at Basin Scale, Water Resources Research, 57, https://doi.org/10.1029/2020WR028390, 2021.

Pinault, J.-L., Amraoui, N., and Golaz, C.: Groundwater-Induced Flooding in Macropore-Dominated Hydrological System in the Context of Climate Changes, Water Resources Research, 41, https://doi.org/10.1029/2004WR003169, 2005.

Price, M., Low, R. G., and McCann, C.: Mechanisms of Water Storage and Flow in the Unsaturated Zone of the Chalk Aquifer, Journal of Hydrology, 233, 54–71, https://doi.org/10.1016/S0022-1694(00)00222-5, 2000.

Prudhomme, C., Hannaford, J., Harrigan, S., Boorman, D., Knight, J., Bell, V., Jackson, C., Svensson, C., Parry, S., Bachiller-Jareno, N., Davies, H., Davis, R., Mackay, J., McKenzie, A., Rudd, A., Smith, K., Bloomfield, J., Ward, R., and Jenkins, A.: Hydrological Outlook UK: An Operational Streamflow and Groundwater Level Forecasting System at Monthly to Seasonal Time Scales, Hydrological Sciences Journal, 62, 2753–2768, https://doi.org/10.1080/02626667.2017.1395032, 2017.

Quintana-Seguí, P., Moigne, P. L., Durand, Y., Martin, E., Habets, F., Baillon, M., Canellas, C., Franchisteguy, L., and Morel, S.: Analysis of Near-Surface Atmospheric Variables: Validation of the SAFRAN Analysis over France, Journal of Applied Meteorology and Climatology, 47, 92–107, https://doi.org/10.1175/2007JAMC1636.1, 2008.

Rakovec, O., Samaniego, L., Hari, V., Markonis, Y., Moravec, V., Thober, S., Hanel, M., and Kumar, R.: The 2018–2020 Multi-Year Drought Sets a New Benchmark in Europe, Earth's Future, 10, e2021EF002 394, https://doi.org/10.1029/2021EF002394, 2022.

Ramos, M.-H., Bartholmes, J., and Thielen-del Pozo, J.: Development of Decision Support Products Based on Ensemble Forecasts in the European Flood Alert System, Atmospheric Science Letters, 8, 113–119, https://doi.org/10.1002/asl.161, 2007.

Rasmussen, J., Madsen, H., Jensen, K. H., and Refsgaard, J. C.: Data Assimilation in Integrated Hydrological Modeling Using Ensemble Kalman Filtering: Evaluating the Effect of Ensemble Size and Localization on Filter Performance, Hydrol. Earth Syst. Sci., 19, 2999–3013, https://doi.org/10.5194/hess-19-2999-2015, 2015.

Rasmussen, J., Madsen, H., Jensen, K. H., and Refsgaard, J. C.: Data Assimilation in Integrated Hydrological Modelling in the Presence of Observation Bias, Hydrol. Earth Syst. Sci., 20, 2103–2118, https://doi.org/10.5194/hess-20-2103-2016, 2016.

Revel, M., Ikeshima, D., Yamazaki, D., and Kanae, S.: A Physically Based Empirical Localization Method for Assimilating Synthetic SWOT Observations of a Continental-Scale River: A Case Study in the Congo Basin, Water, 11, 829, https://doi.org/10.3390/w11040829, 2019.

Saleh, F., Flipo, N., Habets, F., Ducharne, A., Oudin, L., Viennot, P., and Ledoux, E.: Modeling the Impact of In-Stream Water Level Fluctuations on Stream-Aquifer Interactions at the Regional Scale, Journal of Hydrology, 400, 490–500, https://doi.org/10.1016/j.jhydrol.2011.02.001, 2011.

Scargle, J. D.: Studies in Astronomical Time Series Analysis. II-Statistical Aspects of Spectral Analysis of Unevenly Spaced Data, The Astrophysical Journal, 263, 835–853, http://articles.adsabs.harvard.edu/full/1982ApJ...263..835S, 1982.

Shukla, S. and Lettenmaier, D. P.: Seasonal Hydrologic Prediction in the United States: Understanding the Role of Initial Hydrologic Conditions and Seasonal Climate Forecast Skill, Hydrology and Earth System Sciences, 15, 3529–3538, https://doi.org/10.5194/hess-15-3529-2011, 2011.

Stahl, K., Kohn, I., Blauhut, V., Urquijo, J., De Stefano, L., Acácio, V., Dias, S., Stagge, J. H., Tallaksen, L. M., Kampragou, E., Van Loon, A. F., Barker, L. J., Melsen, L. A., Bifulco, C., Musolino, D., de Carli, A., Massarutto, A., Assimacopoulos, D., and Van Lanen, H. A. J.: Impacts of European Drought Events: Insights from an International Database of Text-Based Reports, Natural Hazards and Earth System Sciences, 16, 801–819, https://doi.org/10.5194/nhess-16-801-2016, 2016.

https://doi.org/10.5194/egusphere-2026-1504
Preprint. Discussion started: 18 May 2026

Sun, L., Seidou, O., Nistor, I., and Liu, K.: Review of the Kalman-type Hydrological Data Assimilation, Hydrological Sciences Journal, 61, 2348–2366, https://doi.org/10.1080/02626667.2015.1127376, 2016.

Surdyk, N., Thiéry, D., Nicolas, J., Gutierrez, A., Vigier, Y., and Mougin, B.: MétéEAU Nappes: A Real Time Water Resource Management Tool and Its Application to a Sandy Aquifer in a High Demand Irrigation, Hydrogeology Journal, https://doi.org/10.1007/s10040-022-02509-1, 2022.

Tang, Q., Delottier, H., Kurtz, W., Nerger, L., Schilling, O. S., and Brunner, P.: HGS-PDAF (Version 1.0): A Modular Data Assimilation Framework for an Integrated Surface and Subsurface Hydrological Model, Geoscientific Model Development, 17, 3559–3578, https://doi.org/10.5194/gmd-17-3559-2024, 2024.

Thiéry, D.: Forecast of Changes in Piezometric Levels by a Lumped Hydrological Model, Journal of Hydrology, 97, 129–148, https://doi.org/10.1016/0022-1694(88)90070-4, 1988.

Thiéry, D.: Groundwater Flow Modeling in Porous Media Using MARTHE, in: Modeling Software, edited by Tanguy, J.-M., chap. 4, pp. 45–62, John Wiley & Sons, Ltd, ISBN 978-1-118-55789-1, https://doi.org/10.1002/9781118557891.ch4, 2013.

Thiéry, D.: Logiciel EROS Version 7.1. Guide d'utilisation, Tech. Rep. BRGM/RP-67704-FR, http://infoterre.brgm.fr/rapports/RP-67704-FR.pdf, 2018.

Thiéry, D. and Moutzopoulos, C.: Un modèle hydrologique spatialisé pour la simulation de très grands bassins: le modèle EROS formé de grappes de modèles globaux élémentaires., in: VIIIèmes journées hydrologiques de l'ORSTOM : Régionalisation en hydrologie, application au développement, pp. 285–295, Montpellier, France, https://hal.science/hal-01061971/, 1992.

Thiéry, D., Amraoui, N., and Noyer, M.-L.: Modelling Flow and Heat Transfer through Unsaturated Chalk – Validation with Experimental Data from the Ground Surface to the Aquifer, Journal of Hydrology, 556, 660–673, https://doi.org/10.1016/j.jhydrol.2017.11.041, 2018.

Thiéry, D., Picot-Colbeaux, G., and Guillemoto, Q.: Guidelines for MARTHE v7.8 Computer Code for Hydro-Systems Modelling (English Version), Tech. Rep. BRGM/RP-69660-FR, BRGM, http://ficheinfoterre.brgm.fr/document/RP-69660-FR, 2020.

Thirel, G., Martin, E., Mahfouf, J.-F., Massart, S., Ricci, S., Regimbeau, F., and Habets, F.: A Past Discharge Assimilation System for Ensemble Streamflow Forecasts over France – Part 2: Impact on the Ensemble Streamflow Forecasts, Hydrology and Earth System Sciences, 14, 1639–1653, https://doi.org/10.5194/hess-14-1639-2010, 2010.

Tripathy, K. P. and Mishra, A. K.: How Unusual Is the 2022 European Compound Drought and Heatwave Event?, Geophysical Research Letters, 50, e2023GL105 453, https://doi.org/10.1029/2023GL105453, 2023.

Van Loon, A. F., Van Huijgevoort, M. H. J., and Van Lanen, H. a. J.: Evaluation of Drought Propagation in an Ensemble Mean of Large-Scale Hydrological Models, Hydrology and Earth System Sciences, 16, 4057–4078, https://doi.org/10.5194/hess-16-4057-2012, 2012.

Vergnes, J.-P., Roux, N., Habets, F., Ackerer, P., Amraoui, N., Besson, F., Caballero, Y., Courtois, Q., de Dreuzy, J.-R., Etchevers, P., Gallois, N., Leroux, D. J., Longuevergne, L., Le Moigne, P., Morel, T., Munier, S., Regimbeau, F., Thiéry, D., and Viennot, P.: The AquiFR Hydrometeorological Modelling Platform as a Tool for Improving Groundwater Resource Monitoring over France: Evaluation over a 60-Year Period, Hydrology and Earth System Sciences, 24, 633–654, https://doi.org/10.5194/hess-24-633-2020, 2020.

Verma, K., Munier, S., Boone, A., and Le Moigne, P.: CTRIP-HyDAS: A Global-Scale Data Assimilation Framework for SWOT-Derived Discharge Using Synthetic Observations at High Resolution (1/12°), Water Resources Research, 62, e2025WR040 888, https://doi.org/10.1029/2025WR040888, 2026.

Vidal, J.-P., Martin, E., Franchistéguy, L., Baillon, M., and Soubeyroux, J.-M.: A 50-Year High-Resolution Atmospheric Reanalysis over France with the Safran System, International Journal of Climatology, 30, 1627–1644, https://doi.org/10.1002/joc.2003, 2010.

https://doi.org/10.5194/egusphere-2026-1504
Preprint. Discussion started: 18 May 2026

Virtanen, P., Gommers, R., Oliphant, T. E., Haberland, M., Reddy, T., Cournapeau, D., Burovski, E., Peterson, P., Weckesser, W., Bright, J., van der Walt, S. J., Brett, M., Wilson, J., Millman, K. J., Mayorov, N., Nelson, A. R. J., Jones, E., Kern, R., Larson, E., Carey, C. J., Polat, İ., Feng, Y., Moore, E. W., VanderPlas, J., Laxalde, D., Perktold, J., Cimrman, R., Henriksen, I., Quintero, E. A., Harris, C. R., Archibald, A. M., Ribeiro, A. H., Pedregosa, F., and van Mulbregt, P.: SciPy 1.0: Fundamental Algorithms for Scientific Computing in Python, Nature Methods, 17, 261–272, https://doi.org/10.1038/s41592-019-0686-2, 2020.

Vossepoel, F. C., Evensen, G., and van Leeuwen, P. J.: Adaptive Correlation- and Distance-Based Localization for Iterative Ensemble Smoothers in a Coupled Nonlinear Multiscale Model, Monthly Weather Review, 153, 2593–2609, https://doi.org/10.1175/MWR-D-24-0269.1, 2025.

Wada, Y., van Beek, L. P. H., van Kempen, C. M., Reckman, J. W. T. M., Vasak, S., and Bierkens, M. F. P.: Global Depletion of Groundwater Resources, Geophysical Research Letters, 37, https://doi.org/10.1029/2010GL044571, 2010.

Wada, Y., Wisser, D., and Bierkens, M. F. P.: Global Modeling of Withdrawal, Allocation and Consumptive Use of Surface Water and Groundwater Resources, Earth System Dynamics, 5, 15–40, https://doi.org/10.5194/esd-5-15-2014, 2014.

Wanders, N., Thober, S., Kumar, R., Pan, M., Sheffield, J., Samaniego, L., and Wood, E. F.: Development and Evaluation of a Pan-European Multimodel Seasonal Hydrological Forecasting System, Journal of Hydrometeorology, 20, 99–115, https://doi.org/10.1175/JHM-D-18-0040.1, 2019.

West, L. J., Farrell, R. P., Foley, A. E., Howlett, P. R., and Massei, N.: An Introduction to the Chalk Aquifers of Northern Europe, Geological Society, London, Special Publications, 517, SP517–2023–3, https://doi.org/10.1144/SP517-2023-3, 2023.

White, J. T.: A Model-Independent Iterative Ensemble Smoother for Efficient History-Matching and Uncertainty Quantification in Very High Dimensions, Environmental Modelling & Software, 109, 191–201, https://doi.org/10.1016/j.envsoft.2018.06.009, 2018.

Willemet, J.-M., Munier, S., Besson, F., Etchevers, P., Le Moigne, P., Rousset, F., Soubeyroux, J.-M., Viel, C., Habets, F., Ackerer, P., Amraoui, N., de Dreuzy, J.-R., Gallois, N., Magand, C., Thiéry, D., and Vergnes, J.-P.: Aqui-FR: Towards a Hydro-Geological Seasonal Forecasting System for Metropolitan France, in: IAHS-AISH Scientific Assembly, vol. IAHS2022-525, Copernicus Meetings, Montpellier, France, https://doi.org/10.5194/iahs2022-525, 2022.

Winckel, A., Ollagnier, S., and Gabillard, S.: Managing Groundwater Resources Using a National Reference Database: The French ADES Concept, SN Applied Sciences, 4, 217, https://doi.org/10.1007/s42452-022-05082-0, 2022.

Zhang, D., Madsen, H., Ridler, M. E., Refsgaard, J. C., and Jensen, K. H.: Impact of Uncertainty Description on Assimilating Hydraulic Head in the MIKE SHE Distributed Hydrological Model, Advances in Water Resources, 86, 400–413, https://doi.org/10.1016/j.advwatres.2015.07.018, 2015.

Zhang, D., Madsen, H., Ridler, M. E., Kidmose, J., Jensen, K. H., and Refsgaard, J. C.: Multivariate Hydrological Data Assimilation of Soil Moisture and Groundwater Head, Hydrology and Earth System Sciences, 20, 4341–4357, https://doi.org/10.5194/hess-20-4341-2016, 2016.

Zhou, H., Gómez-Hernández, J. J., and Li, L.: Inverse Methods in Hydrogeology: Evolution and Recent Trends, Advances in Water Resources, 63, 22–37, https://doi.org/10.1016/j.advwatres.2013.10.014, 2014.